Geol. Mag. **155** (*1*), *2018, pp. 132–148.* © *Cambridge University Press 2017*
doi:10.1017/S0016756817000577

Early Jurassic adakitic rocks in the southern Lhasa sub-terrane, southern Tibet: petrogenesis and geodynamic implications

XINFANG SHUI*‡, ZHENYU HE*§†, REINER KLEMD§, ZEMING ZHANG*, TIANYU LU*¶ & LILI YAN*§¶

*Institute of Geology, Chinese Academy of Geological Sciences, Beijing 100037, China
‡School of Earth Sciences, China University of Geosciences, Wuhan 430074, China
§GeoZentrum Nordbayern, Universität Erlangen, Schlossgarten 5a, 91054 Erlangen, Germany
¶School of Earth Sciences and Resources, China University of Geosciences, Beijing 100083, China

(*Received* 11 February 2017; *accepted* 5 June 2017; *first published online* 2 August 2017)

Abstract – Cretaceous–Miocene adakitic rocks in the southern Lhasa sub-terrane have been intensively investigated, while possible Early Jurassic adakitic rocks in this area have been largely neglected. Petrological and geochemical studies revealed adakitic affinities of an Early Jurassic quartz diorite intrusion with mafic enclaves and three tonalite bodies from the Jiacha area in the southern Lhasa sub-terrane. Laser ablation inductively coupled plasma mass spectrometry (LA-ICP-MS) zircon U–Pb dating suggests crystallization ages of 199–179 Ma for these rocks. Both quartz diorites and tonalites have typical adakitic geochemical characteristics such as high Al_2O_3 (15.14–18.22 wt. %) and Sr (363–530 ppm) contents, low Y (4.46–15.9 ppm) and Yb (0.51–1.74 ppm) contents and high Sr/Y ratios of 27–106. The adakitic quartz diorites are further characterized by high MgO (2.63–3.46 wt. %), $Mg^{\#}$ (48–54) and $\varepsilon_{Hf}(t)$ (6.6–13.4) values, which were probably produced by partial melting of a subducted oceanic slab with a mantle contribution. The adakitic tonalites have very low abundances of compatible elements and relatively low $\varepsilon_{Hf}(t)$ values (3.5–10.3), and are interpreted to have formed by partial melting of Neoproterozoic mafic lower crust. Upwelling asthenosphere, triggered by rollback of the subducting Bangong–Nujiang (Meso-Tethys) oceanic plate, provided the necessary heat for slab and lower crust melting, resulting in the geochemical diversity of the coexisting felsic intrusive rocks. Contrary to other models, this study further demonstrates that the Bangong–Nujiang oceanic plate was subducted southward beneath the Lhasa terrane during the Early Jurassic.

Keywords: Adakitic rocks, slab melting, Early Jurassic, Bangong–Nujiang (Meso-Tethys) Ocean, southern Lhasa sub-terrane

1. Introduction

The origin of adakitic rocks, which are characterized by $SiO_2 \geq 56$ wt. %, $Al_2O_3 \geq 15$ wt. %, Sr ≥ 400 ppm, Sr/Y ≥ 20, Y ≤ 18 ppm and Yb ≤ 1.9 ppm according to the definition of Defant & Drummond (1990), is a matter of continuous discussion in the geoscientific community. Originally adakitic lavas, occurring in fore-arc environments, were interpreted as typical melting products of very young (<25 Ma) subducted oceanic crust (Defant & Drummond, 1990, 1993). However, in 'cold' subduction zones, relatively old oceanic crust usually follows *P–T* paths with low geothermal gradients of *c.* 5–7 °C km^{-1}, thereby preventing melting at shallow depths (e.g. Peacock, Rushmer & Thompson, 1994; Peacock *et al.* 2005; Kimura, Kasahara & Takeda, 2009). Therefore, the presence of adakitic igneous rocks in several fore-arc environments above former 'cold' subduction zones (e.g. Nakamura & Iwamori, 2013) led to several alternative tectonogenetic models such as the subduction of the leading edges of newly subducted slabs (Sajona *et al.* 1993; Yogodzinski *et al.* 2001) or slab-window margins (Thorkelson & Breitsprecher, 2005), slab tearing (Pallares *et al.* 2007; Calmus *et al.* 2011), highly oblique convergence (Yogodzinski & Kelemen, 1998), and flat subduction (Gutscher *et al.* 2000) to account for the melting of old oceanic crust beneath fore-arc regions. Furthermore, due to the occurrence of adakitic igneous rocks, which are not the result of slab melting, various geodynamic models have been suggested to explain their petrogenesis (see Castillo, 2006, 2012; Ribeiro, Maury & Grégoire, 2016): (1) melting of mafic, fertilized mantle-derived materials underplated at the base of lower crust (e.g. Atherton & Petford, 1993; Guo, Wilson & Liu, 2007; Zhao *et al.* 2008); (2) high-pressure mineral fractionation of mantle-derived wet basaltic magmas (Castillo, Janney & Solidum, 1999; Garrison & Davidson, 2003; MacPherson, Dreher & Thirlwall, 2006; Rodriguez *et al.* 2007; Petrone & Ferrari, 2008; Gao *et al.* 2009); and (3) mixing and mingling of evolved melts with mantle melts in shallower crustal storage regions, periodically refluxed by mantle melts (e.g. Castillo, Janney & Solidum, 1999; Ribeiro, Maury & Grégoire, 2016).

Mesozoic–Cenozoic magmatic rocks are widespread in the southern Lhasa sub-terrane (Fig. 1; Schärer, Xu & Allegre, 1984; Coulon *et al.* 1986;

†Author for correspondence: ahhzy@163.com.

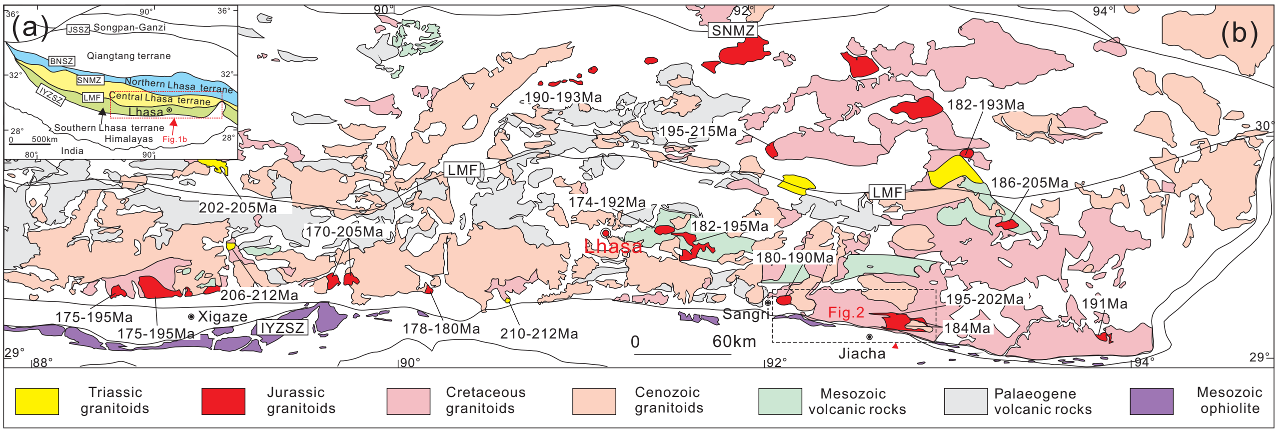

Figure 1. (Colour online) (a) Tectonic framework of south Tibet, showing major tectonic subdivisions (modified from Zhu *et al.* 2011*a*). (b) Geological map of the Gangdese belt (modified from Mo *et al.* 2013), showing the distributions and ages of Late Triassic–Early Jurassic intrusive rocks (age data are from Chu *et al.* 2006; Liu *et al.* 2006; Qu, Xin & Xu, 2007; Zhang *et al.* 2007*a*, *b*; Ji *et al.* 2009*a*, *b*; Yang *et al.* 2011; Zhu *et al.* 2011*a*; Dong & Zhang, 2013; Guo *et al.* 2013; Qiu *et al.* 2015; Meng *et al.* 2016*a*, *b*; Shui *et al.* 2016; Ma *et al.* 2017). Abbreviations: JSSZ = Jinshajiang Suture Zone; BNSZ = Bangong–Nujiang Suture Zone; SNMZ = Shiquan River–Nam Tso Mélange Zone; LMF = Luobadui–Milashan Fault; IYZSZ = Indus–Yarlung Zangbo Suture Zone.

Chung *et al.* 2003; Mo *et al.* 2005; Chu *et al.* 2006; Wen *et al.* 2008*a*, *b*; Ji *et al.* 2009*a*, *b*, 2012; Zhu *et al.* 2009, 2011*a*, 2015; Mo, 2011; Ma *et al.* 2013, 2014; Qiu *et al.* 2015). Among them, Cretaceous–Miocene (137–10 Ma) adakitic rocks have been recognized and intensively investigated (e.g. Chung *et al.* 2003; Hou *et al.* 2004; Gao *et al.* 2007, 2010; Guo, Wilson & Liu, 2007; Wen *et al.* 2008*a*; Zhu *et al.* 2009; Guan *et al.* 2010, 2012; Zhang *et al.* 2010; Chen *et al.* 2011; Ji *et al.* 2012; Jiang *et al.* 2012; Zheng *et al.* 2012; Ma *et al.* 2013, 2014; Meng *et al.* 2014; Xu *et al.* 2015). The Cretaceous adakitic rocks in the southern Lhasa sub-terrane are believed to be a result of partial melting of the subducted Neo-Tethyan oceanic plate or of partial melting of thickened lower crust in response to the subduction of the Neo-Tethyan oceanic plate (Wen *et al.* 2008*a*; Zhu *et al.* 2009; Guan *et al.* 2010; Zhang *et al.* 2010; Jiang *et al.* 2012; Ma *et al.* 2013; Xu *et al.* 2015). The Cenozoic adakitic rocks were suggested to have formed by partial melting of thickened lower mafic crust, subducted oceanic crust or metasomatized mantle during the India–Asia collision (Chung *et al.* 2003; Hou *et al.* 2004; Gao *et al.* 2007, 2010; Guo, Wilson & Liu, 2007; Guan *et al.* 2012; Ji *et al.* 2012; Ma *et al.* 2014; Meng *et al.* 2014). Typically, the Cenozoic adakitic rocks were thought to indicate the timing of the crustal thickening of the Tibetan Plateau as well as the subduction of the Indian continent beneath the Lhasa terrane (Chung *et al.* 2003; Hou *et al.* 2004; Guo, Wilson & Liu, 2007; Guan *et al.* 2012; Ji *et al.* 2012; Ma *et al.* 2014; Meng *et al.* 2014). In contrast, the presence of Early Jurassic adakitic rocks is poorly documented in the southern Lhasa sub-terrane.

Furthermore, a long-standing controversy exists as to whether the Late Triassic–Early Jurassic igneous rocks are the products of partial melting of underplated mafic lower crust or of ancient continental crust (Chu *et al.* 2006; Zhang *et al.* 2007*a*, *b*; Yang *et al.* 2011; Zhu *et al.* 2011*a*; Dong & Zhang, 2013; Guo *et al.* 2013; Meng *et al.* 2016*a*, *b*; Shui *et al.* 2016; Ma *et al.* 2017). Therefore, the study of the largely neglected Early Jurassic adakitic rocks will provide important information on their petrogenesis and tectonic setting in the southern Lhasa sub-terrane.

In this paper, we present petrological, geochemical, zircon U–Pb and Hf isotopic data of the Early Jurassic adakitic rocks and associated mafic enclaves from the Jiacha area in order to constrain their petrogenesis and discuss the Early Jurassic tectonic evolution of the southern Lhasa sub-terrane.

2. Geological background and petrography

The Lhasa terrane is bounded by the Bangong–Nujiang suture zone to the north and the Indus–Yarlung Tsangpo suture zone to the south, representing Meso- and Neo-Tethys ocean relics, respectively (Fig. 1a; Yin & Harrison, 2000). It is generally divided into southern, central and northern sub-terranes, which are separated by the Luobadui–Milashan Fault (LMF) and the Shiquanhe–Nam Tso Mélange Zone (SNMZ) (Fig. 1a; Zhu *et al.* 2011*a*). The Bangong–Nujiang ocean (Meso-Tethys) is believed to have subducted southward beneath the Lhasa terrane during the Permian to the Early Cretaceous (e.g. Pan *et al.* 2004; Qiu *et al.* 2004; Zhu *et al.* 2011*a*). However, Kapp *et al.* (2003, 2007) suggested a northward subduction beneath the Qiangtang terrane in the Late Jurassic.

The southern Lhasa sub-terrane mainly consists of juvenile crust with Precambrian basement slivers (e.g. Mo, 2011; Ji *et al.* 2009*a*; Zhu *et al.* 2011*a*, *b*). This sub-terrane comprises the Gangdese belt, which extends ~2500 km from east to west (Fig. 1b; Mo *et al.* 2005; Chu *et al.* 2006; Ji *et al.* 2009*a*, *b*; Mo, 2011). It consists of large-scale intrusive complexes and widespread volcanic rocks, which were mainly generated

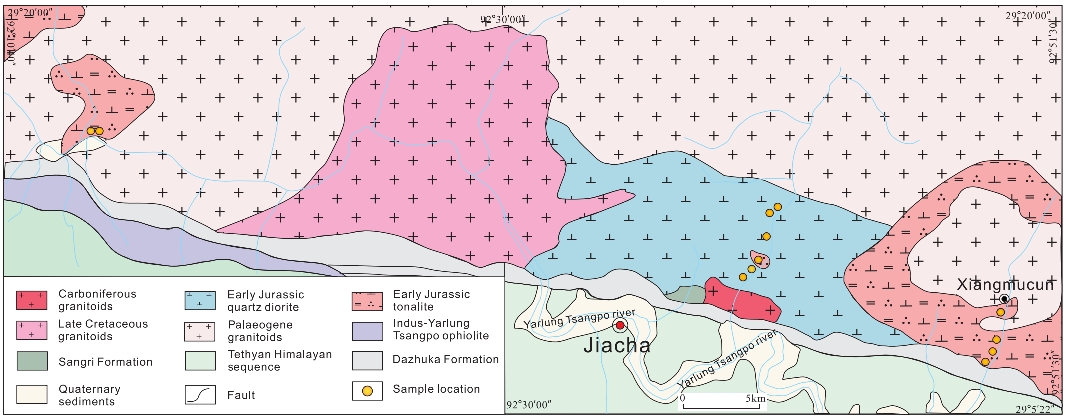

Figure 2. (Colour online) Geological map of the Jiacha area, eastern Gangdese belt.

between 220 Ma and 13 Ma (Fig. 1a; Yin & Harrison, 2000; Chung *et al*. 2003; Mo *et al*. 2005, 2011; Chu *et al*. 2006; Wen *et al*. 2008*a*, *b*; Zhu *et al*. 2008, 2009, 2011*a*; Ji *et al*. 2009*a*, *b*, 2012; Kang *et al*. 2014; Meng *et al*. 2016*a*, *b*). These igneous rocks show two age peaks of ~109–80 Ma and ~65–41 Ma (Ji *et al*. 2009*a*, *b*; Zhu *et al*. 2011*a*). The Late Triassic –Early Jurassic intrusions (215–182 Ma) mainly consist of intermediate-silicic rocks (Chu *et al*. 2006; Liu *et al*. 2006; Qu, Xin & Xu, 2007; Zhang *et al*. 2007*a*, *b*; Ji *et al*. 2009*a*, *b*; Zhu *et al*. 2011*a*; Dong & Zhang, 2013; Guo *et al*. 2013; ; Meng *et al*. 2016*a*, *b*; Ma *et al*. 2017), with coeval volcanic rocks of the Sangri Group (Kang *et al*. 2014) and the Yeba Formation (Zhu *et al*. 2008; Wei, 2014).

The studied Early Jurassic quartz diorite and tonalite rocks were collected in the Jiacha area in the eastern part of the Gangdese belt (Fig. 2). Middle Carboniferous, Late Cretaceous and Palaeogene granitoids are also exposed in this area (Fig. 2; Ji *et al*. 2009*b*, 2012; Dong & Zhang, 2013). The quartz diorite has an exposure area of *c*. 60 km^2 and is distinctly elongated in an approximately E–W direction (Fig. 2). The subspherical to irregular mafic enclaves (5–35 cm in diameter) are randomly distributed in the quartz diorite (Fig. 3a, b). They have sharp to gradational contacts with the host quartz diorite. Plagioclase phenocrysts cross-cut the interface between the mafic enclaves and the host quartz diorite (Fig. 3b). The tonalites were collected from three different intrusive bodies, which cross-cut the quartz diorite in places (Figs 2, 3c, d). A summary of the sample locations and the petrographical features is given in Table 1.

The quartz diorite, which displays a weak mylonitic foliation in places, is medium-grained and mainly consists of plagioclase (55–60 vol. %), amphibole (10–15 vol. %), quartz (~15 vol. %), biotite (~10 vol. %), minor K-feldspar (~2 vol. %) and accessory magnetite, titanite, apatite and zircon (Fig. 4a). Andesitic plagioclase is 1.0–3.0 mm in length (An = 32–50; Supplementary Table S1, available at https://doi.org/10.1017/S0016756817000577) (Fig. 4a). The euhedral to subhedral amphibole is commonly interstitial, sometimes poikilitic, enclosing plagioclase and oxides, and partly altered to chlorite and epidote (Fig. 4a). The mafic enclaves contain 2–3 mm long plagioclase phenocrysts (An = 39–68) in a matrix of fine- to medium-grained plagioclase (40–55 vol. %), amphibole (20–30 vol. %), biotite (~5 vol. %) and quartz (~5 vol. %) with minor K-feldspar and needle-like apatite (Fig. 4b, c).

The small tonalite body intruding the quartz diorite (Fig. 2) is fine-grained and mainly consists of plagioclase (~60 vol. %), quartz (~30 vol. %), biotite (~3 %) and minor K-feldspar (Fig. 4d). Plagioclase exhibits typical oscillatory zoning (Fig. 4d). Samples GD14-50-1 and GD14-50-2 are collected from a tonalite body near Sangri, to the west of the Jiacha area (Figs 1, 2). They are medium-grained, weakly mylonitized and mainly consist of plagioclase (55–60 vol. %), quartz (25–30 vol. %), biotite (~5 vol. %), amphibole (~5 vol. %) and minor K-feldspar (Fig. 4e). The tonalite body near Xiangmucun is medium-grained and consists of plagioclase (An = 30–50; 50–60 vol. %), quartz (20–25 vol. %), biotite (3–10 vol. %) and minor amphibole and K-feldspar, with accessory zircon and apatite (Figs 2, 3d, 4f).

3. Analytical methods

The chemical composition of plagioclase was determined using a JEOL JXA 8800R microprobe with a 20 kV accelerating voltage and a 20 nA beam current at the Institute of Mineral Resources, Chinese Academy of Geological Sciences (CAGS), Beijing. The representative microprobe analytical results are listed in Supplementary Table S1.

Zircon grains were extracted using standard density and magnetic separation techniques. Cathodoluminescence (CL) images of analysed zircon grains were obtained using an FEI NOVA NanoSEM 450 scanning electron microscope equipped with a Matan Mono CL4 cathodoluminescence system at the Institute of Geology, CAGS. Zircon U–Pb dating was carried out using a laser ablation inductively coupled plasma mass spectrometer (LA-ICP-MS; Perkin Elmer Elan DRC

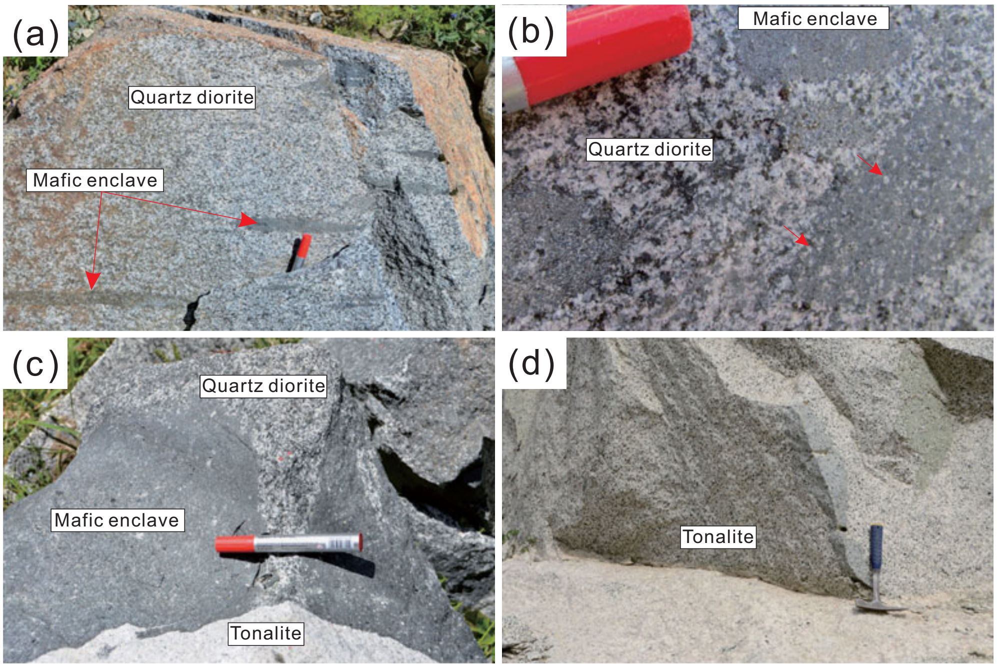

Figure 3. (Colour online) Field photos of the Jiacha Early Jurassic adakitic intrusions. (a) The quartz diorite contains elongated mafic enclaves. (b) Ellipsoidal, spindle-shaped mafic enclaves in the host quartz diorite. Note that some crystals cross-cut the boundary between host rock and enclave. Plagioclase phenocrysts are indicated with red arrows. (c) The tonalite intrudes the quartz diorite. (d) The tonalite outcrop lies in the Xiangmucun area, east of Jiacha.

Table 1. Ages, lithologies and major mineral assemblages of the Jiacha Early Jurassic adakitic rocks.

Sample	Age (Ma)	Lithology	Major mineral assemblage	GPS position
GD14-89-1	198 ± 4	Quartz diorite	Pl + Amp + Qtz + Bi	N29° 12′ 57″; E92° 41′ 34″
GD14-93-1	199 ± 4		Pl + Amp + Qtz + Bi	N29° 10′ 13″; E92° 40′ 07″
GD14-90-3	198 ± 3	Mafic enclave in quartz diorite	Pl + Amp + Bi + Qtz	N29° 12′ 19″; E92° 41′ 13″
GD15-L09-2	196 ± 3		Pl + Amp + Bi + Qtz	N29° 10′ 56″; E92° 40′ 54″
GD15-L08-1	198 ± 2	Tonalite intruding the quartz diorite	Pl + Qtz + Kfs + Bi	N29° 10′ 37″; E92° 40′ 32″
GD14-50-1	179 ± 2	Tonalite near the Sangri	Pl + Qtz + Kfs + Bi + Amp	N29° 15′ 05″; E92° 13′ 31″
GD14-99-2	184 ± 4	Tonalite near the Xiangmucun	Pl + Qtz + Kfs + Bi + Amp	N29° 09′ 05″; E92° 50′ 35″
GD14-102-2	184 ± 4		Pl + Qtz + Kfs + Bi + Amp	N29° 07′ 43″; E92° 50′ 18″

Abbreviations: Amp =amphibole; Bi = biotite; Kfs = K-feldspar; Pl = plagioclase; Qtz = quartz.

II) equipped with a Microlas system (GeoLas 200 M, 193 nm ArFexcimer laser) at the Key Laboratory of Crust–Mantle Materials and Environments of CAS at the University of Science and Technology of China.

Zircon 91500 and SRM610 were used as external standards for the U–Pb isotope ratios and the trace element analysis, respectively. Details of the instrument parameters and analysis procedures are given in Liu *et al.* (2007). The spot diameter of the laser ablation pits is 32 μm. Details of the instrument parameters and analysis procedures are given in Liu *et al.* (2007) and Gu *et al.* (2013). The LaDating (version 1.5) software was used for processing the U/Pb data. The quantitative calibration for the Pb isotope dating was performed by ComPbcorr#3_18 (Andersen, 2002). The age calculations and concordia diagrams (data-point error ellipses are 68.3 % conf.) were performed using Isoplot/Ex_ver3 (Ludwig, 2003).

Zircon Lu–Hf isotopic analyses were carried out *in situ* using a Neptune Plus multi-collector inductively coupled plasma mass spectrometer (MC-ICP-MS) in combination with a Geolas 2005 excimer ArF laser ablation system at the State Key Laboratory of Geological Processes and Mineral Resources, China University of Geosciences (Wuhan). The energy density of the laser ablation was 5.3 J cm^{-2} and the ablation spot was 44 μm in diameter. Zircons 91500, GJ-1, Mud Tank and Temora were analysed as reference standards. Detailed operating conditions for the laser ablation system and the MC-ICP-MS instrument and analytical procedures are similar to those described by Hu *et al.* (2012). Off-line selection and integration of analysis signals, and mass bias calibrations were performed using ICPMSDataCal (Liu *et al.* 2010). The measured $^{176}Lu/^{177}Hf$ ratios and the ^{176}Lu decay constant of 1.867×10^{-11} a^{-1} (Söderlund *et al.* 2004) were used to calculate initial $^{176}Hf/^{177}Hf$ ratios. The Chondritic values of $^{176}Lu/^{177}Hf = 0.0336$ and $^{176}Hf/^{177}Hf = 0.282785$ reported by Bouvier, Vervoort & Patchett, (2008) were used to calculate the εHf values. The depleted mantle Hf model ages (T_{DM}) were calculated using the

https://doi.org/10.1017/S0016756817000577 Published online by Cambridge University Press

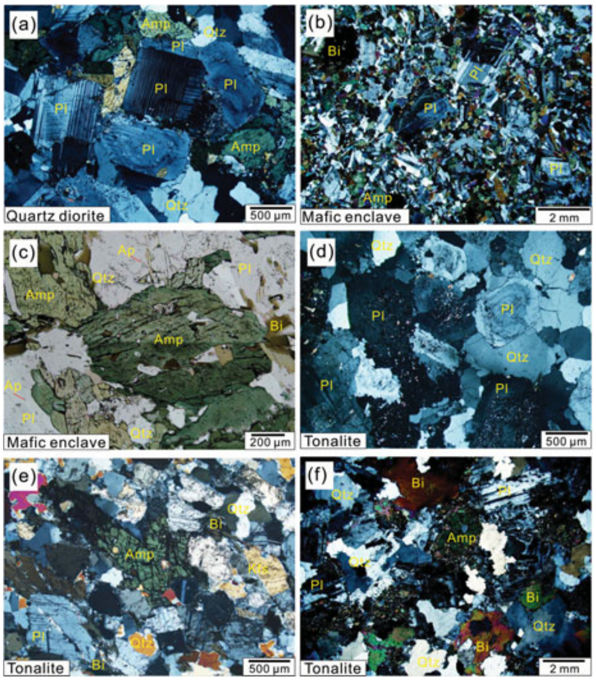

Figure 4. (Colour online) Photomicrographs of the Jiacha Early Jurassic adakitic intrusions. (a) The quartz diorite consists mainly of plagioclase, amphibole and quartz. (b) The mafic enclave of quartz diorite consists of plagioclase phenocrysts and fine-grained plagioclase, amphibole and biotite. (c) Amphibole from mafic enclave contains plagioclase, quartz and biotite inclusions; also showing the needle-like apatite. (d) The tonalite mainly consists of plagioclase and quartz (GD15-L08-1). (e) The tonalite mainly consists of plagioclase, quartz, biotite, amphibole and minor K-feldspar (GD14-50-1). (f) The tonalite from Xiangmucun mainly consists of plagioclase, quartz, minor K-feldspar, biotite and some amphibole (GD14-102-1). (a, b, d, e, f) Crossed polarized light. (c) Plane polarized light. Abbreviations: Amp = amphibole; Pl = plagioclase; Bi = biotite; Ap = apatite; Qtz = quartz.

measured $^{176}Lu/^{177}Hf$ ratios based on the assumption that the depleted mantle reservoir has a linear isotopic growth from $^{176}Hf/^{177}Hf = 0.279718$ at 4.55 Ma to 0.283250 at present, with $^{176}Lu/^{177}Hf = 0.0384$ (Griffin *et al*. 2000). Two-stage model ages (T_{DM2}) were calculated by assuming that the parental magma was produced from an average continental crust ($^{176}Lu/^{177}Hf = 0.015$) (Griffin *et al*. 2002).

The whole-rock major- and trace-element compositions were analysed at the National Research Centre for Geoanalysis, CAGS. The whole-rock major elements were performed using X-ray fluorescence (XRF, PW4400) with an analytical uncertainty of <2 %. Trace-element abundances were measured by inductively coupled plasma mass spectrometry (ICP-MS, PE300D), which gives a precision better than 10 % for most of the elements analysed.

4. Results

4.a. Whole-rock major and trace elements

Whole-rock major and trace elements of the Jiacha Early Jurassic igneous rocks are listed in Supplementary Table S2. All samples are sub-alkaline in the total alkali–silica (TAS) diagram (Fig. 5a). The quartz diorite samples have variable SiO_2 (58–63 wt. %) and high Al_2O_3 (>16 %), MgO (2.63–3.46 wt. %), Na_2O/K_2O (>2) and $Mg^{\#}$ (48–54) values. They are metaluminous with A/CNK [molar $Al_2O_3/(CaO + Na_2O + K_2O)$] ratios of 0.87–0.93 and plot in the medium-K calc-alkaline series field on the K_2O vs SiO_2 diagram (Fig. 5b, c). In the PRIMA-normalized spidergram (Fig. 6a) these rocks show a strong enrichment of large-ion lithophile elements (LILEs) and pronounced negative Nb, Ta and Ti anomalies. Furthermore, they display slightly negative Eu anomalies (Eu/Eu* = 0.83–0.92) and have inclined chondrite-normalized rare earth element (REE) patterns (Fig. 6b), while $(La/Yb)_N$ ranges from 3.90 to 7.93. In addition, they have relatively low heavy rare earth element (HREE) (Yb = 1.09–1.74 ppm) and Y concentrations (10.4–15.9 ppm), as well as high Sr contents (412–504 ppm) and Sr/Y ratios (29.2–45.1). Therefore these rocks have an adakitic character according to the definition of Defant & Drummond (1990, 1993), which is also revealed by using the Sr/Y vs Y discrimination diagram (Fig. 5d).

The mafic enclaves in the quartz diorites have SiO_2 contents of 52–53 wt. %, MgO contents of 4.82–5.72 wt. % and an $Mg^{\#}$ of 51–58. In the PRIMA-normalized spidergram (Fig. 6a), they exhibit a relative enrichment in LILEs (e.g. Rb, K and Pb). Their REE patterns are mildly fractionated with $(La/Yb)_N$ of 3.3–3.7 and slightly negative Eu anomalies (Eu/Eu* = 0.81–0.90) in the chondrite-normalized spidergram (Fig. 6b). The REE concentrations are rather high (Yb = 2.56–2.62 ppm and Y = 21.5–28.0 ppm) compared to those of the host quartz diorites, and plot in the island-arc field on the Sr/Y vs Y discrimination diagram (Fig. 5d).

The tonalite samples have high SiO_2 (64–70 wt. %) and total alkali ($K_2O + Na_2O = 5.04$–6.07 wt. %) concentrations and low MgO (0.93–2.25 wt. %) and P_2O_5 (0.07–0.15 wt. %) contents compared to those of the quartz diorite samples. According to the K_2O vs SiO_2 diagram, the samples belong to the medium-K series (Fig. 5b) and are metaluminous to slightly peraluminous, with A/CNK ratios of 0.93–1.08 (Fig. 5c). The samples show strong enrichments of LILEs and pronounced negative Nb–Ta–Ti anomalies in the PRIMA-normalized spidergrams (Fig. 6c). They further display fractionated REE patterns with negative to positive Eu anomalies (Eu/Eu* = 0.84–1.43) in the chondrite-normalized spidergram (Fig. 6d). The Sr contents (363–530 ppm), the Sr/Y ratios (27.3–105) as well as the Y (4.46–13.3 ppm) and Yb (95–1.39 ppm) contents are in accordance with the adakite definition as also revealed by the Sr/Y vs Y discrimination diagram (Fig. 5d).

4.b. Zircon U–Pb geochronology

To constrain the timing of the magmatic crystallization events, six samples were selected for LA-ICP-MS

https://doi.org/10.1017/S0016756817000577 Published online by Cambridge University Press

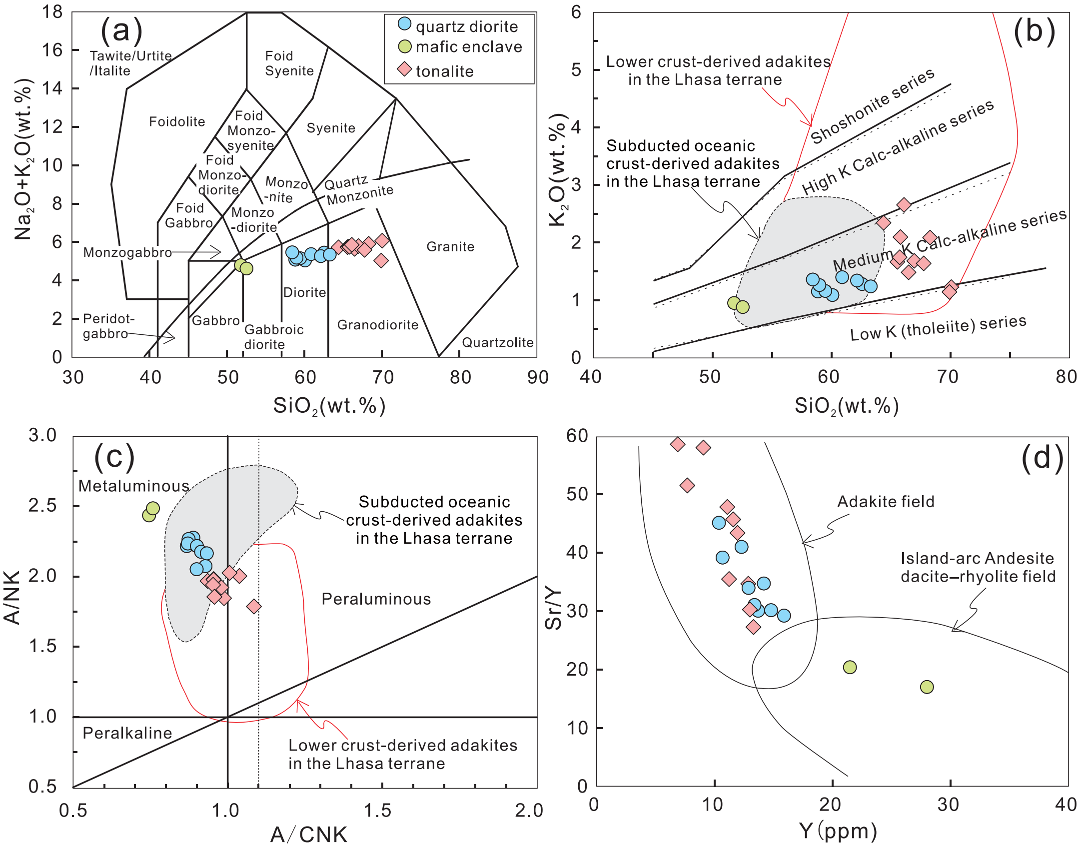

Figure 5. (Colour online) (a) Total alkalis vs silica diagram (after Middlemost, 1994); (b) K_2O vs SiO_2 diagram (after Rollinson, 1993); (c) A/NK vs A/CNK diagram (after Maniar & Piccoli, 1989); (d) Sr/Y vs Y discrimination diagram showing data for adakites and island-arc andesite–dacite–rhyolite rocks (after Defant & Drummond, 1990, 1993). Data sources: Late Cretaceous–Miocene (83–10 Ma) lower crust-derived adakites in the Lhasa terrane (Chung *et al.* 2003; Hou *et al.* 2004; Gao *et al.* 2007, 2010; Guo, Wilson & Liu, 2007; Wen *et al.* 2008*a*; Guan *et al.* 2012; Ma *et al.* 2014; Meng *et al.* 2014). Cretaceous (137–86 Ma) subducted oceanic crust-derived adakites in the Lhasa terrane (Zhu *et al.* 2009; Guan *et al.* 2010; Zhang *et al.* 2010; Jiang *et al.* 2012; Ma *et al.* 2013).

zircon U–Pb dating. The results are summarized in Table 1 and the data are given in Supplementary Table S3. Zircon grains from the quartz diorite and tonalite samples are euhedral, with crystal lengths of 100–250 μm. They exhibit oscillatory zoning in CL images (Fig. 7a–d), which are typical of magmatic zircon (Hoskin & Schaltegger, 2003). Zircon grains from the mafic enclaves are relatively small (50–100 μm in length) and display broad oscillatory zoning in the CL images (Fig. 7e, f).

Twenty-two analyses on 22 zircon grains from quartz diorite sample GD14-89-1 yield a weighted mean $^{206}Pb/^{238}U$ age of 198 ± 4 Ma (MSWD = 1.5). A further 32 analyses were undertaken on 32 zircon grains from another quartz diorite sample GD14-93-1, which tightly plot on the concordia (Fig. 6b) and give a weighted mean $^{206}Pb/^{238}U$ age of 199 ± 4 Ma (MSWD = 2.0) (Fig. 8a, b). All analyses show variable Th (41–253 ppm) and U (95–365 ppm) contents with Th/U ratios of 0.37–0.86 that are typical for magmatic zircon (Supplementary Table S3).

Twenty-seven spots on 17 zircon grains yield a weighted mean $^{206}Pb/^{238}U$ age of 198 ± 3 Ma (MSWD = 0.8) for the mafic enclave sample GD14-90-3, and 18 spot analyses on 18 zircon grains from sample GD15-L09-2 give a weighted mean $^{206}Pb/^{238}U$ age of 196 ± 3 Ma (MSWD = 2.4), both of which are, within error, identical and are interpreted to represent the crystallization age of the mafic enclave (Fig. 8c, d). All analyses have Th = 40–376 ppm and U = 76–356 ppm with high Th/U ratios of 0.47–1.06 in accordance with magmatic zircon (Supplementary Table S3).

Seventeen U–Pb spots on 17 zircon grains from tonalite sample GD15-L08-1 and 14 U-Pb spots on 14 zircon grains from tonalite sample GD14-50-1 yield weighted mean $^{206}Pb/^{238}U$ ages of 198 ± 2 Ma (MSWD = 2.6) and 179 ± 2 Ma (MSWD = 1.2), respectively (Fig. 8e, f), which are interpreted as the crystallization ages of the tonalites. All analyses have variable Th (38–587 ppm) and U (82–562 ppm) contents and high Th/U ratios of 0.42–1.04 in accordance with magmatic zircon (Supplementary Table S3).

A previous study showed that the Xiangmucun tonalite body has a crystallization age of 184 ± 4 Ma (Table 1; Shui *et al.* 2016). Therefore, the adakitic quartz diorites and tonalites from the Jiacha area of the southern Lhasa sub-terrane were formed in the Early Jurassic (202–179 Ma).

https://doi.org/10.1017/S0016756817000577 Published online by Cambridge University Press

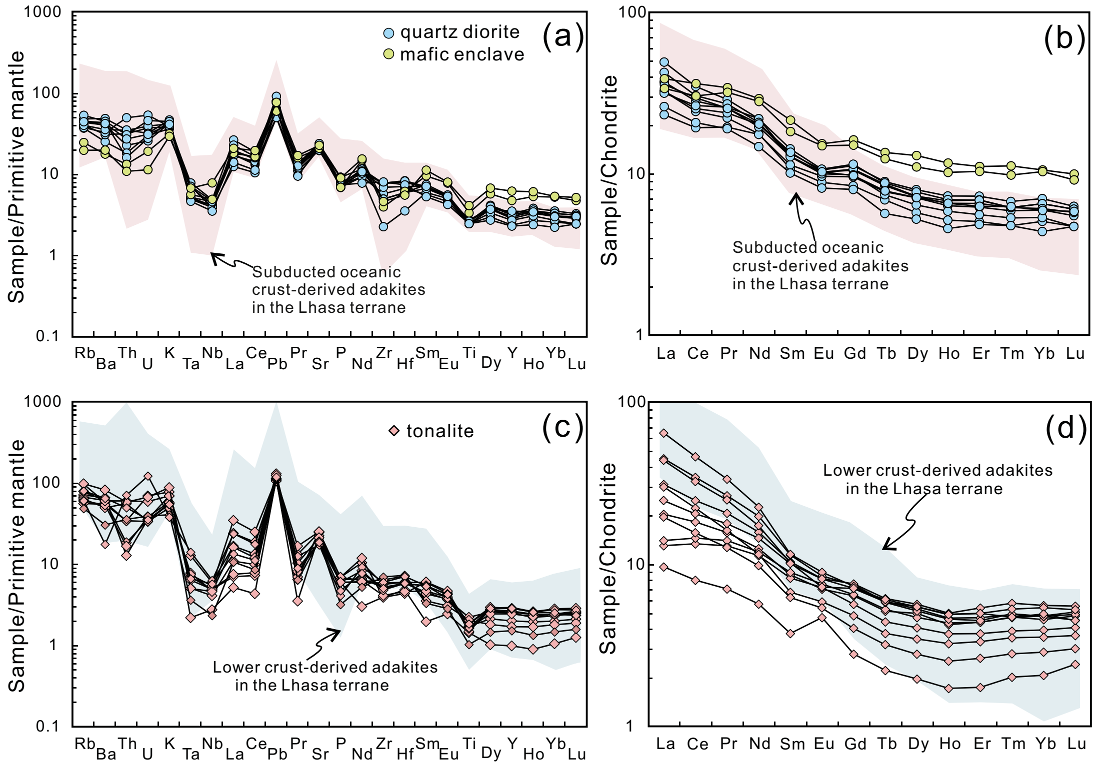

Figure 6. (Colour online) Spider diagrams (a, c) (Sun & McDonough, 1989) and chondrite-normalized REE pattern (b, d) for the Jiacha Early Jurassic adakitic intrusions (Taylor & McLennan, 1985). Adakite fields are shown for comparison. Data sources: Late Cretaceous–Miocene (83–10 Ma) lower crust-derived adakites in the Lhasa terrane (Gao *et al*. 2007; Wen *et al*. 2008*a*; Guan *et al*. 2012; Zheng *et al*. 2012; Ma *et al*. 2014; Meng *et al*. 2014); Cretaceous (137–86 Ma) subducted oceanic crust-derived adakites in the Lhasa terrane (Zhu *et al*. 2009; Zhang *et al*. 2010; Jiang *et al*. 2012; Ma *et al*. 2013).

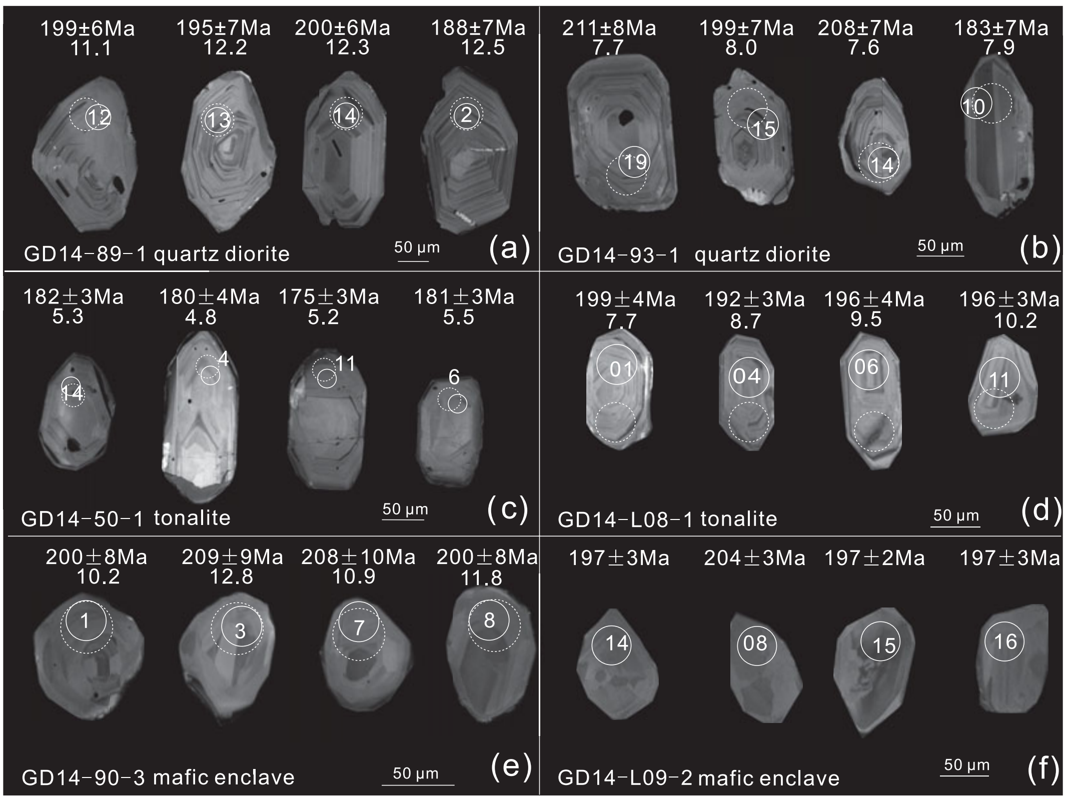

Figure 7. CL images of zircon grains of the Jiacha Early Jurassic adakitic intrusions. Solid and dashed circles indicate the locations of U–Pb dating and Hf isotope analyses, respectively.

https://doi.org/10.1017/S0016756817000577 Published online by Cambridge University Press

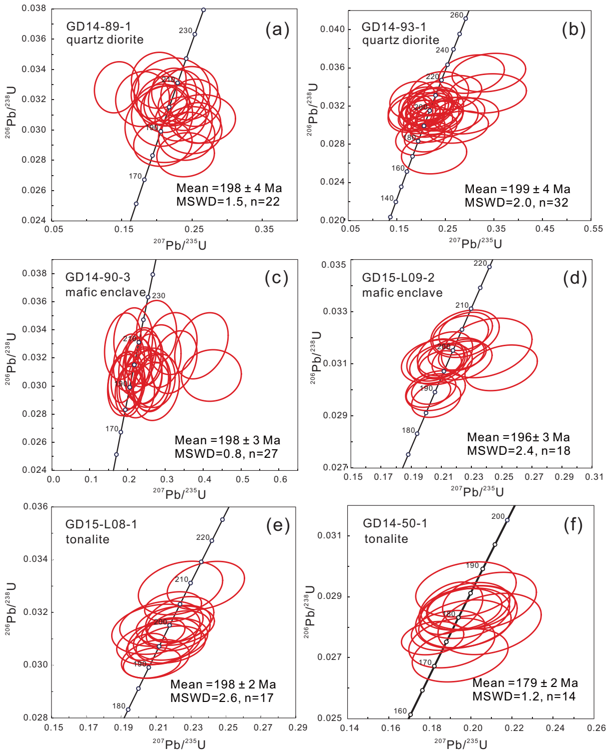

Figure 8. (Colour online) U–Pb concordia diagrams of the Jiacha Early Jurassic adakitic intrusions.

4.c. Zircon Lu–Hf isotope compositions

Zircon grains from two quartz diorite samples (GD14-89-1 and GD14-93-1), two tonalite samples (GD15-L08-1 and GD14-50-1) from different intrusive bodies (Fig. 2) and one mafic enclave sample (GD14-90-3) were analysed for their Lu–Hf isotope compositions. All zircon Hf isotopic spot analyses were performed on the same zircon grains, which were used for the U–Pb dating. The results are given in Supplementary Table S4 and illustrated in Figures 9 and 10.

Fifteen Hf isotopic spot analyses on zircon grains from the quartz diorite sample GD14-89-1 yield initial $^{176}Hf/^{177}Hf$ ratios ranging from 0.282976 to 0.283039, with corresponding $\varepsilon_{Hf}(t)$ values of 11.1–13.4 (Figs 9a, 10) and two-stage Hf model ages of 503–359 Ma. Fifteen Hf isotopic spot analyses on the zircon grains from the other sample (GD14-93-1) yield initial $^{176}Hf/^{177}Hf$ ratios of 0.282846–0.282955, with relatively low $\varepsilon_{Hf}(t)$ values of 6.6–10.5 (Figs 9b, 10) and high two-stage Hf model ages ranging from 798 to 548 Ma.

Fifteen Hf isotopic spot analyses on zircon grains from the mafic enclave sample (GD14-90-3) yield a narrow range of $\varepsilon_{Hf}(t)$ values of 10.0–13.0 with corresponding two-stage Hf crustal model ages of 577–385 Ma (Figs 9c, 10).

Fourteen Hf isotopic analyses on zircon grains from the tonalite sample GD15-L08-1 show initial $^{176}Hf/^{177}Hf$ ratios of 0.282867–0.282952 and corresponding $\varepsilon_{Hf}(t)$ values of 7.3–10.3, while two-stage Hf model ages range from 750 to 555 Ma (Figs 9d, 10). Fifteen Hf isotopic analyses on zircon grains from the tonalite sample GD14-50-1 show a narrow $\varepsilon_{Hf}(t)$ value range of 3.5–5.5 and two-stage Hf crustal model ages of 977–850 Ma (Figs 9e, 10).

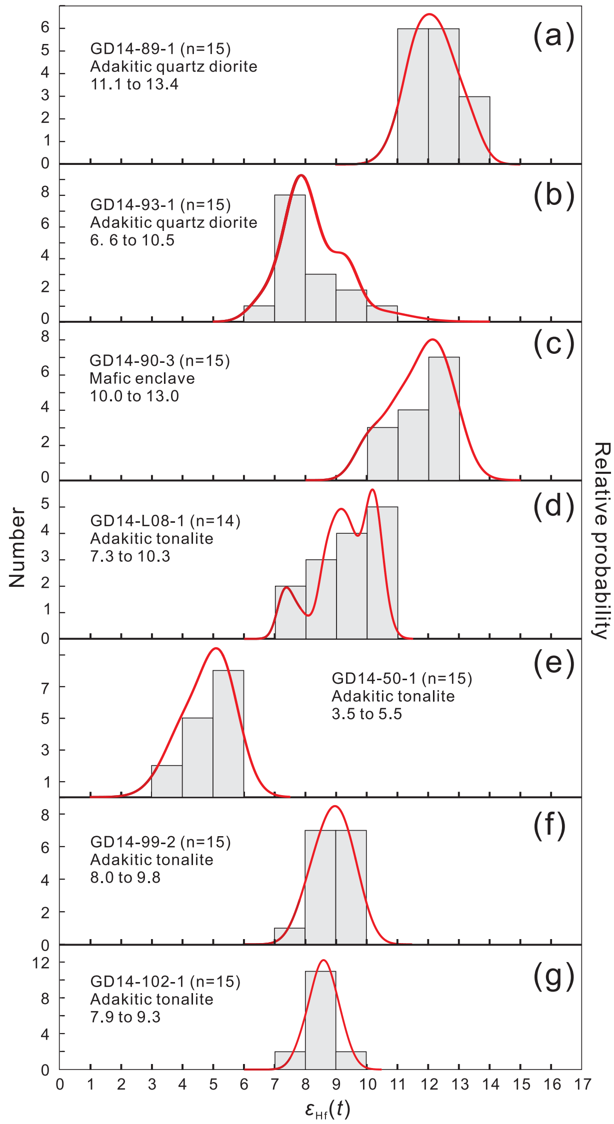

Figure 9. (Colour online) Histograms of zircon $\varepsilon_{Hf}(t)$ values of the Jiacha Early Jurassic adakitic intrusions. The data of samples GD14-99-2 and GD14-102-1 are from Shui *et al.* (2016).

Shui *et al.* (2016) obtained Hf isotopic compositions for two samples (GD14-99-2 and GD14-102-1) from the Xiangmucun tonalite in a previous study. One sample GD14-99-2 has zircon $\varepsilon_{Hf}(t)$ values of 8.0–9.8 and two-stage Hf model age of 695–575 Ma (Figs 9f, 10), while the other sample GD14-102-1 yields similar zircon $\varepsilon_{Hf}(t)$ values of 7.9–9.3 and two-stage Hf model ages of 700–610 Ma (Figs 9g, 10).

5. Discussion

5.a. Magma mixing process: the mafic enclaves in the quartz diorite

Mafic enclaves are quite common in granitoids and can provide important information on the origin of the host rocks and related geodynamic processes (e.g.

https://doi.org/10.1017/S0016756817000577 Published online by Cambridge University Press

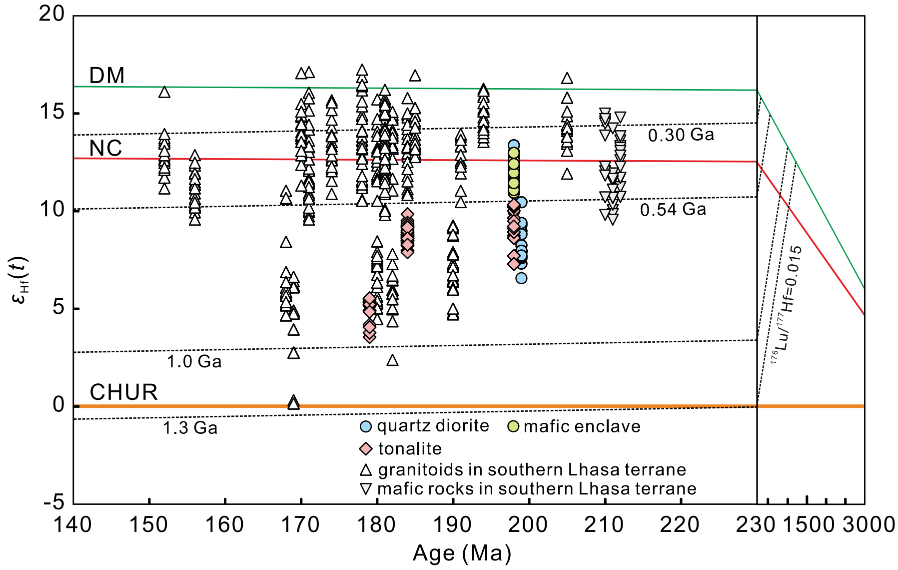

Figure 10. (Colour online) Plot of zircon $\varepsilon_{Hf}(t)$ values vs U–Pb ages of the Jiacha Early Jurassic adakitic intrusions. Data sources: Granitoids in southern Lhasa terrane (Zhang *et al.* 2007*a*; Ji *et al.* 2009*a*, *b*; Yang *et al.* 2011; Zhu *et al.* 2011*a*; Dong & Zhang, 2013; Guo *et al.* 2013; Meng *et al.* 2016*a*); mafic rocks in southern Lhasa terrane (Meng *et al.* 2016*b*). The new continental crust (NC) evolutionary line is defined by isotopic growth from $^{176}Hf/^{177}Hf = 0.279703$ at 4.55 Ga to 0.283145 at present, with $^{176}Lu/^{177}Hf = 0.0375$ (Dhuime, Hawkesworth & Cawood, 2011).

Vernon, 1984; Chappell, White & Wyborn, 1987; Barbarin, 2005; Mo *et al.* 2005; Yang *et al.* 2007; Gao *et al.* 2009; Shellnutt, Jahn & Dostal, 2010; Wang *et al.* 2012; Meng *et al.* 2014; Lu *et al.* 2016). Several possibilities were proposed for the formation of the enclaves, including xenoliths from the country rock (e.g. Xu *et al.* 2006), cumulates of early-formed co-genetic crystals (e.g. Gao *et al.* 2009; Shellnutt, Jahn & Dostal, 2010; Niu *et al.* 2013; Chen *et al.* 2015), refractory and residual phase assemblages of the sources of the granitoids (e.g. Chappell, White & Wyborn, 1987), and products of magma mixing and mingling (Vernon, 1984; Barbarin, 2005; Mo *et al.* 2005; Yang *et al.* 2007; Meng *et al.* 2014; Lu *et al.* 2016). In the last model, the mafic enclaves are believed to have formed by a mafic magma intruding a felsic magma chamber, where they mixed and mingled (Vernon, 1984; Barbarin, 2005; Yang *et al.* 2007).

Here, oval or irregular-shaped mafic enclaves are abundant in the host quartz diorite (Fig. 3a–c) and both types have, within error, identical U–Pb zircon magmatic crystallization ages (Fig. 8a–d). The mafic enclaves contain euhedral acicular apatites enclosed within the larger plagioclase grains (Fig. 4c), corresponding with a typical rapid quenching texture (Sparks & Marshall, 1986). Some plagioclase phenocrysts in the mafic enclaves seem to be transferred from the host magma (Figs 3b, 4a, b), which is thought to be due to the low rheological contrast between the two magmas that allows crystal transfer from a more felsic host magma into a more mafic magma (Waight, Maas & Nicholls, 2000; Perugini *et al.* 2003). Amphiboles in such mafic enclaves are commonly characterized by inclusions of quartz, biotite, Fe–Ti oxides and needle-like apatite, also indicating magma mixing (Foley *et al.* 2013; Lu *et al.* 2016) (Fig. 4b, c). Therefore, the mafic enclaves in the Jiacha quartz diorites are thought to represent globules of mafic magmas that were injected and mixed with the colder, partially crystallized host magma (e.g. Wang *et al.* 2012).

The mafic enclaves are medium-K calc-alkaline rocks that are relatively enriched in LILE and depleted in HFSE with negative Nb, Ta and Ti anomalies (Figs 5a, b, 6b). The depleted Hf isotopic values ($\varepsilon_{Hf}(t) = 10.0$–13.0) of the mafic enclaves are similar to those of contemporaneous gabbroic rocks (215 Ma) in the southern Lhasa sub-terrane (Fig. 10), which were interpreted to have formed in the metasomatized mantle wedge (Meng *et al.* 2016*b*). The mafic enclaves exhibit Nb/Ta ratios ranging from 15.1 to 20.2 that are similar to or slightly higher than those (15.5–17.4) of the primitive and depleted mantle and chondrite (Barth *et al.* 2000). This indicates that the primitive magma of the mafic enclaves originated from metasomatized mantle peridotites.

5.b. Adakitic quartz diorites: partial melting of subducted oceanic crust

As noted above, the Jiacha quartz diorite has adakitic affinities, e.g. high Al_2O_3 (16.60–18.22 wt.%), Sr (412–504 ppm), Sr/Y (29.2–45.1), low Y (10.4–15.9 ppm) and Yb (1.09–1.74 ppm) and slightly negative Eu anomalies (Figs 5d, 6a, b). Adakitic rocks may be generated by a variety of mechanisms (see above). We propose that the studied Jiacha adakitic quartz diorite probably formed by partial melting of subducting oceanic crust based on the following reasons: (1) The Jiacha adakitic quartz diorite has low K_2O/Na_2O (0.28–0.35) and high CaO/Al_2O_3 (0.33–0.39) values,

https://doi.org/10.1017/S0016756817000577 Published online by Cambridge University Press

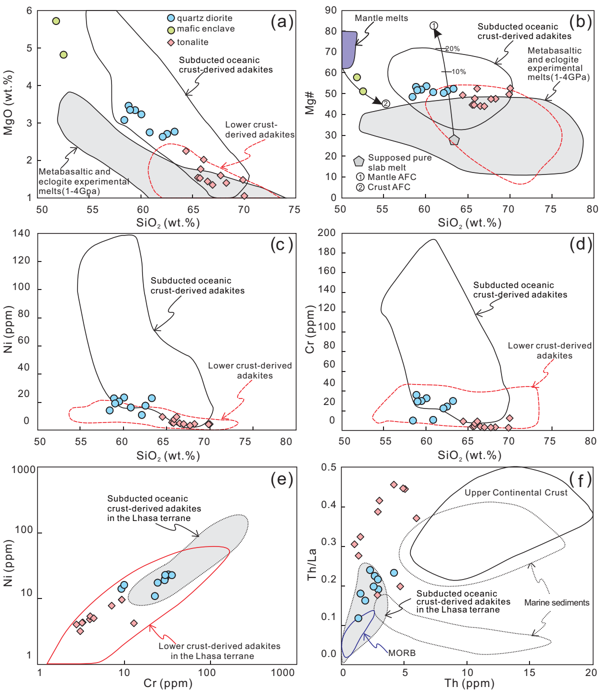

Figure 11. (Colour online) Discrimination diagrams for the Jiacha Early Jurassic adakitic rocks. (a) MgO vs SiO_2 diagram (after Huang *et al*. 2009, and references therein). Data for metabasalt and eclogite experimental melts (1–4 GPa) are from Rapp *et al*. (1999) and references therein; (b) Mg# vs SiO_2 diagram (after Wang *et al*. 2012, and references therein). Mantle AFC curves are after Rapp *et al*. (1999) (curve 1); the proportion of assimilated peridotite is also shown. The crustal AFC curve is after Stern & Kilian (1996) (curve 2); (c) Ni vs SiO_2 diagram (after Huang *et al*. 2009, and references therein); (d) Cr vs SiO_2 diagram (after Huang *et al*. 2009, and references therein); (e) Ni vs Cr diagram. Data sources: Late Cretaceous–Miocene (83–10 Ma) lower crust-derived adakites in the Lhasa terrane (Chung *et al*. 2003; Hou *et al*. 2004; Gao *et al*. 2007, 2010; Guo, Wilson & Liu, 2007; Wen *et al*. 2008*a*; Guan *et al*. 2012; Ma *et al*. 2014; Meng *et al*. 2014). Cretaceous (137–86 Ma) subducted oceanic crust-derived adakites in the Lhasa terrane (Zhu *et al*. 2009; Guan *et al*. 2010; Zhang *et al*. 2010; Jiang *et al*. 2012; Ma *et al*. 2013); (f) Th/La vs Th diagram. The data for upper continental crust are from Plank (2005) and references therein. The data for marine sediments are from Plank & Langmuir (1998) and for MORB are from Niu & Batiza (1997).

which are similar to those of adakitic rocks generated by partial melting of subducted oceanic crust (with $K_2O/Na_2O < 0.71$ and $CaO/Al_2O_3 > 0.2$), including the Cretaceous adakites from the southern Lhasa subterrane (Fig. 5b, c; Stern & Kilian, 1996; Li *et al*. 2016). Furthermore, the Jiacha adakitic quartz diorite samples mostly plot in the field of adakitic rocks derived from melting of subducting oceanic crust in the Ni, Cr, Mg# and MgO discrimination diagrams (Fig. 11 a–e). The high MgO and Mg# values may indicate the interaction of a slab-derived adakitic melt and a mantle-derived magma which is also supported by the presence of the mafic enclaves (Sen & Dunn, 1994; Rapp *et al*. 1999). As shown in the SiO_2 vs Mg# diagram (Fig. 11b), mantle AFC modelling (DePaolo, 1981) indicates that the Jiacha adakitic melts most likely mixed with a small amount (< 10 %) of mantle-derived magma (Hofmann, 1988); (2) The HREE and Y contents, and the Sr/Y, $(La/Yb)_N$ and $(Dy/Yb)_N$ ratios of the quartz diorite are generally consistent with those of the Cretaceous adakites derived from subducted oceanic crust in the southern Lhasa sub-terrane (Fig. 6a, b). Their relatively low $(La/Yb)_N$ ratios may also have resulted from interaction with a mantle-derived magma. Furthermore, their Th and Th/La values are similar to those of the Cretaceous slab-derived adakites in the southern Lhasa sub-terrane (Fig. 11f; Zhu *et al*. 2009; Zhang *et al*. 2010; Jiang *et al*. 2012; Ma *et al*. 2013); and (3) The $\varepsilon_{Hf}(t)$ values of the Jiacha adakitic quartz diorite display positive zircon $\varepsilon_{Hf}(t)$ values (6.6–13.4) (Fig. 9), which are similar to those of Indian Ocean MORB (Chauvel & Blichert-Toft, 2001). Furthermore at least half of the values plot near the ‘new continental crust’ evolutionary line (Dhuime, Hawkesworth & Cawood, 2011) (Fig. 10), implying significant involvement of newly formed juvenile crustal material.

In summary, the Jiacha adakitic quartz diorite was probably derived by partial melting of subducting oceanic crust. The slab-derived melts were mixed with mantle-derived magma during ascent, which increased their MgO and compatible elements contents. It is noteworthy that sample GD14-93-01 shows lower $\varepsilon_{Hf}(t)$ values (6.6–10.5) than the other quartz diorite sample ($\varepsilon_{Hf}(t) = 11.1$–13.4) (Figs 9, 10). This indicates that crustal-derived magma may also have contributed to the generation of the adakitic quartz diorites, which is also consistent with their low Ni and Cr contents relative to the typical slab-derived melts (Fig. 11c, d) and is similar to a modified slab-derived magma modified by crustal components (Kelemen, Hart & Bernstein, 1998).

5.c. Adakitic tonalites: partial melting of thickened lower crust

Although the adakitic quartz diorite and tonalites coexist in the southern Lhasa sub-terrane, there is a disparity in their geochemical characters, indicating different magma sources (Figs 5, 6, 11). The adakitic tonalites have high SiO_2, K_2O and low A/NK ratios, MgO (0.93–2.25 wt. %) and Mg# (44–53) values are similar to those of experimentally derived metabasaltic and eclogitic melts at high pressures of 1.0–4.0 GPa and adakitic rocks derived from thickened lower crust (Fig. 5b, c; Fig. 11a, b). Melting experiments have revealed that pristine melts of basaltic rocks yield low MgO and Mg# values (e.g. Rapp & Watson, 1995), which are similar to those of adakitic rocks derived from partial melting of thickened lower crust (Castillo, 2012). In the Ni vs Cr and Cr vs SiO_2 diagrams (Fig. 11c–e), all tonalite samples plot in the field of Late Cretaceous–Miocene adakitic rocks derived by partial melting of thickened lower crust from the southern Lhasa sub-terrane, which is in accordance with the very low concentrations of compatible elements

https://doi.org/10.1017/S0016756817000577 Published online by Cambridge University Press

(Cr = 2.71–13.0 ppm, Ni = 3.12–9.60 ppm; Fig. 11e). Therefore, we suggest that the Jiacha adakitic tonalites were probably derived by partial melting of thickened lower crust.

The concave-upward Dy–Ho–Er–Tm-depleted patterns (Fig. 6d) observed in the Jiacha adakitic tonalites indicate that they were probably formed by partial melting of basaltic lower crust under variable water fugacities, generating a garnet-bearing and amphibole-rich residue (Petford & Atherton, 1996; Guan *et al.* 2012; Shui *et al.* 2016). However, garnet is strongly enriched in HREE, while amphibole is relatively enriched in MREE (Green, 1994). The Jiacha adakitic tonalite samples show stronger depletions of MREE than HREE, suggesting that amphibole is the major residual phase rather than garnet.

The adakitic tonalites have lower $\varepsilon_{Hf}(t)$ (3.5–10.3) values relative to those of the adakitic quartz diorite (Fig. 9). All samples plot in the evolutionary zone of the Neoproterozoic crust below the 'new continental crust' evolutionary line (Dhuime, Hawkesworth & Cawood, 2011) (Fig. 10), implying that the Jiacha adakitic tonalites were probably formed by reworking of Neoproterozoic mafic lower crust (Figs 9, 10). However, the tonalites from the different bodies have inconsistent Hf isotopic compositions, with some high $\varepsilon_{Hf}(t)$ values close to those of the quartz diorites (Figs 9, 10), indicating that the Neoproterozoic mafic lower crust cannot have acted alone as their single melt source but rather represent mixing products of highly differentiated crustal and mantle-derived melts. Therefore, the heterogeneous zircon Hf isotopic compositions of the adakitic quartz diorites and tonalites of the southern Lhasa sub-terrane indicate extensive melt interaction involving slab-, mantle- and ancient crustal-derived melts. The Jiacha adakitic tonalites were probably derived by partial melting of Neoproterozoic mafic lower crust in the stability field of garnet and amphibole with variable contributions of mantle- or slab-derived magma.

5.d. Tectonic implications for the Bangong–Nujiang Ocean (Meso-Tethys) subduction

Recently, voluminous Late Triassic–Early Jurassic intrusive rocks (226–150 Ma) including mafic rocks and normal calc-alkaline granitoids were discovered in the southern Lhasa sub-terrane (e.g. Chu *et al.* 2006; Qu, Xin & Xu, 2007; Zhang *et al.* 2007*a*; Ji *et al.* 2009*a*, *b*; Yang *et al.* 2011; Zhu *et al.* 2011*a*; Dong & Zhang, 2013; Guo *et al.* 2013; Qiu et al. 2015; Meng *et al.* 2016*a*, *b*; Shui *et al.* 2016; Ma *et al.* 2017) (Fig. 1b). The mafic rocks were interpreted to be products of partial melting of a heterogeneous mantle source (Kang *et al.* 2014; Meng *et al.* 2016*b*). Normally calc-alkaline granitoids are metaluminous to peraluminous, with concave-upward MREE-depleted REE patterns, and their magmas are thought to have dominantly formed by partial melting of juvenile lower crust with variable ancient continental crustal material contributions (Chu *et al.* 2006; Zhang *et al.* 2007*a*; Ji *et al.* 2009*a*, *b*; Zhu *et al.* 2011*a*; Guo *et al.* 2013; Meng *et al.* 2016*a*). These Late Triassic–Early Jurassic magmatic rocks are interpreted to have formed in an arc tectonic setting (Zhang *et al.* 2007*a*; Zhu *et al.* 2008; Ji *et al.* 2009*a*, *b*; Kang *et al.* 2014; Meng *et al.* 2016*a*, *b*; Wang *et al.* 2016). However, two contrasting tectonic models have mainly been proposed for the formation of the Late Triassic–Early Jurassic arc setting: (1) northward subduction of the Neo-Tethyan oceanic plate (e.g. Chu *et al.* 2006; Zhang *et al.* 2007*a*, *b*; Zhu *et al.* 2008; Guo *et al.* 2013; Kang *et al.* 2014; Meng *et al.* 2016*a*, *b*; Wang *et al.* 2016; Ma *et al.* 2017) or (2) southward subduction of the Bangong–Nujiang (Meso-Tethys) oceanic plate (e.g. Zhu *et al.* 2011*a*; Song *et al.* 2014; Wei, 2014; however, see Kapp et al. 2003, 2007 for a different view). The separation of the Lhasa Terrane from northern Australia, resulting from the Neo-Tethyan back-arc spreading, began during mid- to late Triassic times (Metcalfe, 1996, 2009, 2011; Zhu *et al.* 2011*a*, *b*). Furthermore most of the well-studied ophiolites in the Yarlung Zangpo suture zone are 130–120 Ma, suggesting that the initial subduction of the Neo-Tethyan oceanic plate beneath the southern margin of the Lhasa block started in the Cretaceous (at *c.* 130–120 Ma; Zhu *et al.* 2011*a*; Dai *et al.* 2013; Zhong *et al.* 2016). Zhu *et al.* (2011*a*) argued that the Late Triassic–Early Jurassic magmatism of the Lhasa terrane has resulted from the southward Bangong–Nujiang oceanic plate subduction beneath the Lhasa terrane based on a synthesis of Mesozoic–Early Palaeogene magmatic rocks across southern Tibet. The southward-directed Bangong–Nujiang (Meso-Tethys) oceanic plate subduction may have been triggered by the Lhasa–northern Australia collision (Sengör *et al.* 1988; Zhu *et al.* 2011*a*, *b*). Therefore, the Late Triassic–Early Jurassic magmatic rocks in the Lhasa terranes are believed to be related to the southward subduction of the Bangong–Nujiang oceanic plate.

In general, the generation of adakitic magmas from subducting oceanic crust >25 Ma requires an additional heat supply (Defant & Drummond, 1990; Castillio, 2006, 2012). According to experimental results and thermal modelling, partial melting of subducted oceanic crust only occurs in hot subduction zone settings under a restricted set of circumstances (800–1000 °C at depths of 70–80 km: Peacock, Rushmer & Thompson, 1994; Sen & Dunn, 1994; van Keken *et al.* 2011). Thus, a simple normal-angle (cold) subduction model cannot easily explain shallow slab-melting (such as the studied Early Jurassic quartz diorite in the southern Lhasa sub-terrane). This is because at shallow depths of normal subduction zones (i.e. beneath the fore-arc wedge) the dominant fluid-producing process is dehydration instead of melting of the subducted oceanic crust (for an extensive review see Klemd, 2013). Here we suggest that asthenospheric upwelling during the Neo-Tethys back-arc spreading – probably a result of slab rollback of the subducted Meso-Tethys

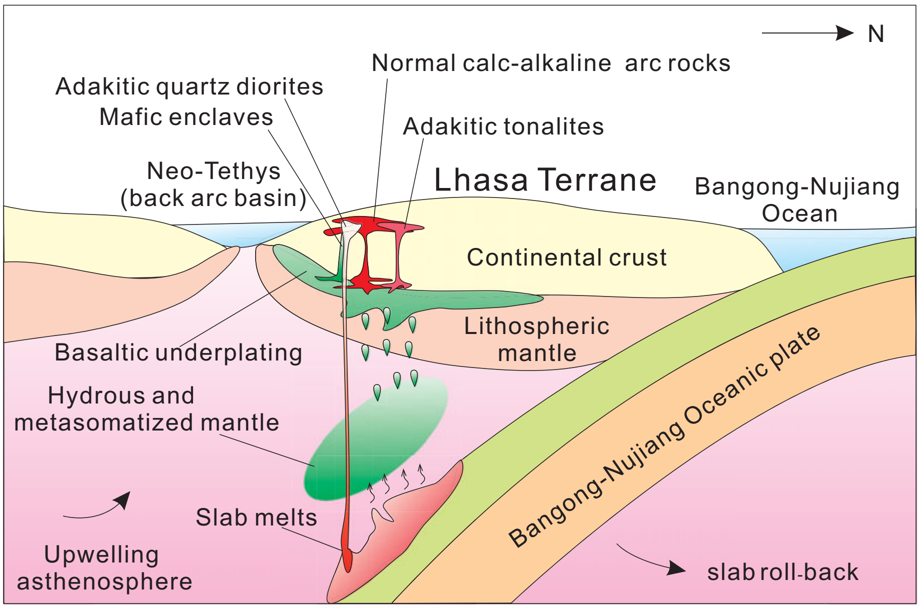

Figure 12. (Colour online) Conceptual diagram illustrating the tectonic and magma genesis of the Lhasa terrane in the Early Jurassic. Slab rollback of the subducted Bangong–Nujiang oceanic plate resulted in hot asthenospheric mantle upwelling and decompression melting as well as initiation of back-arc basin (Neo-Tethys). The asthenospheric upwelling was responsible for high-temperature conditions over a wide area in the fore-arc wedge. The unusually high-temperature conditions in the mantle wedge caused the partial melting of the subducted slab, responsible for formation of the Jiacha adakitic quartz diorites. Synchronously, mantle-derived basaltic magmas were injected into the Jiacha adakitic quartz diorites to form mafic enclaves. Furthermore, the basaltic magma generated by partial melting of the metasomatized mantle wedge underplated the lower crust, resulting in the thickening and reworking of the ancient crust of the southern Lhasa sub-terrane. The adakitic tonalites were produced by partial melting of the thickened lower crust as a result of continued basaltic magma underplating.

oceanic crust – provided the high thermal regime necessary for partial melting of the oceanic crust and was thus responsible for the formation of the Jiacha Early Jurassic adakitic rocks (Fig. 12) (Zhu *et al*. 2011*a*; Song *et al*. 2014; Wei, 2014). The slab rollback is thought to have triggered the invasion of deep asthenosphere into the mantle wedge and the development of an extensional environment in the overlying lithosphere mantle. The high thermal anomaly resulted in the partial melting of the subducted oceanic crust, forming the adakitic quartz diorites. Synchronously, mantle-derived basaltic magmas injected the adakitic quartz diorite to form mafic enclaves. Furthermore, the basaltic magma generated by partial melting of the metasomatized mantle wedge underplated the lower crust, resulting in the thickening and reworking of the ancient crust of the southern Lhasa sub-terrane. Subsequently the adakitic tonalites were produced by partial melting of the thickened lower crust as a result of continued basaltic magma underplating (Fig. 12).

6. Conclusions

(1) LA-ICP-MS zircon U–Pb dating suggests emplacement ages of 199–179 Ma for newly discovered Early Jurassic adakitic rocks from the Jiacha area in the southern Lhasa sub-terrane.

(2) The adakitic quartz diorites are products of partial melting of the subducted Bangong–Nujiang (Meso-Tethys) oceanic crust, while the adakitic tonalites were derived from Neoproterozoic lower crust.

(3) The formation of the Early Jurassic adakitic rocks and Neo-Tethys back-arc spreading probably resulted from slab rollback of the subducted Bangong–Nujiang oceanic plate.

Acknowledgements. This study was supported by National Natural Science Foundation of China (41230205); the Chinese Geological Survey Project (DD20160022); and a scholarship from the China Scholarship Council (Z.Y. H). We thank two anonymous referees for constructive comments on the manuscript, and Dr Chad Deering for editorial handling.

Supplementary material

To view supplementary material for this article, please visit https://doi.org/10.1017/S0016756817000577

References

Andersen, T. 2002. Correction of common lead in U–Pb analyses that do not report ^{204}Pb. *Chemical Geology* **192**, 59–79.

Atherton, M. P. & Petford, N. 1993. Generation of sodium-rich magmas from newly underplated basaltic crust. *Nature* **362**, 144–6.

Barbarin, B. 2005. Mafic magmatic enclaves and mafic rocks associated with some granitoids of the central Sierra Nevada batholith, California: nature, origin, and relations with the hosts. *Lithos* **80**, 155–77.

Barth, M. G., McDonough, W. F. & Rudnick, R. L. 2000. Tracking the budget of Nb and Ta in the continental crust. *Chemical Geology* **165**, 197–213.

Bouvier, A., Vervoort, J. D. & Patchett, P. J. 2008. The Lu–Hf and Sm–Nd isotopic composition of CHUR: constraints from unequilibrated chondrites and implications for the bulk composition of terrestrial planets. *Earth and Planetary Science Letters* **273**, 48–57.

Calmus, T., Pallares, C., Maury, R. C., Aguillón-Robles, A., Bellon, H., Benoit, M. & Michaud, F. 2011. Volcanic markers of the post-subduction evolution of Baja California and Sonora, Mexico: slab tearing versus lithospheric rupture of the Gulf of California. *Pure and Applied Geophysics*, **168**, 1303–30.

Castillo, P. R. 2006. An overview of adakite petrogenesis. *Chinese Science Bulletin* **51**, 257–68.

Castillo, P. R. 2012. Adakite petrogenesis. *Lithos* **134–135**, 304–16.

Castillo, P. R., Janney, P. E. & Solidum, R.U. 1999. Petrology and geochemistry of Camiguin Island, southern Philippines: insights to the source of adakites and other lavas in a complex arc setting. *Contributions to Mineralogy and Petrology* **134**, 33–51.

Chappell, B. W., White, A. J. R. & Wyborn, D. 1987. The importance of residual source material (restite) in granite petrogenesis. *Journal of Petrology* **28**, 1111–38.

Chauvel, C. & Blichert-Toft, J. 2001. A hafnium isotope and trace element perspective on melting of the depleted mantle. *Earth and Planetary Science Letters* **190**, 137–51.

Chen, S., Niu, Y. L., Sun, W. L., Zhang, Y., Li, J. Y., Guo, P. Y. & Sun, P. 2015. On the origin of mafic magmatic enclaves (MMEs) in syn-collisional granitoids: evidence from the Baojishan pluton in the North Qilian Orogen, China. *Mineralogy and Petrology* **109**, 577–96.

Chen, J. L., Xu, J. F., Zhao, W. X., Dong, Y. H., Wang, B. D. & Kang, Z. Q. 2011. Geochemical variations in Miocene adakitic rocks from the western and eastern Lhasa terrane: implications for lower crustal flow beneath the Southern Tibetan Plateau. *Lithos* **125**, 928–39.

Chu, M. F., Chung, S. L., Song, B., Liu, D. Y., O'Reilly, S. Y., Pearson, N. J., Ji, J. Q. & Wen, D. J. 2006. Zircon U–Pb and Hf isotope constraints on the Mesozoic tectonics and crustal evolution of southern Tibet. *Geology* **34**, 745–8.

Chung, S. L., Liu, D. Y., Ji, J. Q., Chu, M. F., Lee, H. Y., Wen, D. J., Lo, C. H., Lee, T. Y., Qian, Q. & Zhang, Q. 2003. Adakites from continental collision zones: melting of thickened lower crust beneath southern Tibet. *Geology* **31**, 1021–4.

Coulon, C., Maluski, H., Bollinger, C. & Wang, S. 1986. Mesozoic and Cenozoic volcanic rocks from central and southern Tibet: ^{39}Ar–^{40}Ar dating, petrological characteristics and geodynamical significance. *Earth and Planetary Science Letters* **79**, 281–302.

Dai, J. G., Wang, C. S., Polat, A., Santosh, M., Li, Y. L. & Ge, Y. K. 2013. Rapid forearc spreading between 130 and 120Ma: evidence from geochronology and geochemistry of the Xigaze ophiolite, southern Tibet. *Lithos* **172–173**, 1–16.

Defant, M. J. & Drummond, M. S. 1990. Derivation of some modern arc magmas by melting of young subducted lithosphere. *Nature* **347**, 662–5.

Defant, M. J. & Drummond, M. S. 1993. Mount St. Helens: potential example of the partial melting of the subducted lithosphere in a volcanic arc. *Geology* **21**, 547–50.

DePaolo, D. J. 1981. Trace element and isotopic effects of combined wallrock assimilation and fractional crystallization. *Earth and Planetary Science Letters* **53**, 189–202.

Dhuime, B., Hawkesworth, C. & Cawood, P. 2011.When continents formed. *Science* **331**, 154–5.

Dong, X. & Zhang, Z. M. 2013. Genesis and tectonic significance of the Early Jurassic magmatic rocks from the southern Lhasa terrane. *Acta Petrologica Sinica* **29**, 1933–48 (in Chinese with English abstract).

Foley, F. V., Pearson, N. J., Rushmer, T., Turner, S. & Adam, J. 2013. Magmatic evolution and magma mixing of Quaternary adakites at Solander and little Solander Islands, New Zealand. *Journal of Petrology* **54**, 703–44.

Gao, J., Klemd, R., Long, L. L., Xiong, X. M. & Qian, Q. 2009. Adakitic signature formed by fractional crystallization: an interpretation for the Neo-Proterozoic meta-plagiogranites of the NE Jiangxi ophiolitic melange belt, South China. *Lithos* **110**, 277–93.

Gao, Y. F., Hou, Z. Q., Kamber, B. S., Wei, R. H., Meng, X. J. & Zhao, R. S. 2007. Adakite-like porphyries from the southern Tibetan continental collision zones: evidence for slab melt metasomatism. *Contributions to Mineralogy and Petrology* **153**, 105–20.

Gao, Y. F., Yang, Z. S., Santosh, M., Hou, Z. Q., Wei, R. H. & Tian, S. H. 2010. Adakitic rocks from slab melt-modified mantle sources in the continental collision zone of southern Tibet. *Lithos* **119**, 651–63.

Garrison, J. M. & Davidson, J. P. 2003. Dubious case for slab melting in the Northern volcanic zone of the Andes. *Geology* **31**, 565–8.

Green, T. H. 1994. Experimental studies of trace-element partitioning applicable to igneous petrogenesis: Sedona 16 years later. *Chemical Geology* **117**, 1–36.

Griffin, W. L., Pearson, N. J., Belousova, E., Jackson, S. E., van Achterbergh, E., O'Reilly, S. Y. & Shee, S. R. 2000. The Hf isotope composition of cratonic mantle: LAM-MC-ICPMS analysis of zircon megacrysts in kimberlites. *Geochimica et Cosmochimica Acta* **64**,133–47.

Griffin, W.L., Wang, X., Jackson, S. E., Pearson, N. J., O'Reilly, S. Y., Xu, X. & Zhou, X. 2002. Zircon chemistry and magma mixing, SE China: in situ analysis of Hf isotopes, Tonglu and Pingtan igneous complexes. *Lithos* **61**, 237–69.

Gu, H. O., Xiao, Y. L., Santosh, M., Li, W. Y., Yang, X. Y., Pack, A. & Hou, Z. H. 2013. Spatial and temporal distribution of Mesozoic adakitic rocks along the Tan-Lu fault, Eastern China: constraints on the initiation of lithospheric thinning. *Lithos* **177**, 352–65.

Guan, Q., Zhu, D. C., Zhao, Z. D., Dong, G. C., Zhang, L. L., Li, X. W., Liu, M., Mo, X. X., Liu, Y. S. & Yuan, H. L. 2012. Crustal thickening prior to 38 Ma in southern Tibet: evidence from lower crust-derived adakitic magmatism in the Gangdese Batholith. *Gondwana Research* **21**, 88–99.

Guan, Q., Zhu, D. C., Zhao, Z. D., Zhang, L. L., Liu, M., Li, X. W., Yu, F., Liu, M. H. & Mo, X. X. 2010. Late Cretaceous adakites from the eastern segment of the Gangdese Belt, Southern Tibet: products of Neo-Tethyan mid-ocean ridge subduction. *Acta Petrologica Sinica* **26**, 2165–79 (in Chinese with English abstract).

Guo, L. S., Liu, Y. L., Liu, S. W., Cawood, P. A., Wang, Z. H. & Liu, H. F. 2013. Petrogenesis of Early to Middle Jurassic granitoid rocks from the Gangdese belt, Southern Tibet: implications for early history of the Neo-Tethys. *Lithos* **179**, 320–33.

Guo, Z. F., Wilson, M. & Liu, J. Q. 2007. Post-collisional adakites in south Tibet: products of partial melting of subduction-modified lower crust. *Lithos* **96**, 205–24.

https://doi.org/10.1017/S0016756817000577 Published online by Cambridge University Press

Gutscher, M. A., Maury, R. & Eissen, J. P., Bourdon, E. 2000. Can slab melting be caused by flat subduction? *Geology* **28**, 535–8.

Hofmann, A. W. 1988. Chemical differentiation of the earth: the relationship between mantle, continental crust, and oceanic crust. *Earth and Planetary Science Letters* **90**, 297–314.

Hoskin, P. W. O. & Schaltegger, U. 2003. The composition of zircon and igneous and metamorphic petrogenesis. *Reviews in Mineralogy and Geochemistry* **53**, 27–62.

Hou, Z. Q., Gao, Y. F., Qu, X. M., Rui, Z. Y. & Mo, X. X. 2004. Origin of adakitic intrusives generated during mid-Miocene east–west extension in southern Tibet. *Earth and Planetary Science Letters* **220**, 139–55.

Hu, Z. C., Liu, Y. S., Gao, S., Liu, W. G., Zhang, W., Tong, X. R., Lin, L., Zong, K. Q., Li, M., Chen, H. H., Zhou, L. & Yang, L. 2012. Improved in situ Hf isotope ratio analysis of zircon using newly designed X skimmer cone and jet sample cone in combination with the addition of nitrogen by laser ablation multiple collector ICP-MS. *Journal of Analytical Atomic Spectrometry* **27**, 1391–9.

Huang, X. L., Xu, Y. G., Lan, J. B., Yang, Q. J. & Luo, Z. Y. 2009. Neoproterozoic adakitic rocks from Mopanshan in the western Yangtze craton: partial melts of a thickened lower crust. *Lithos* **112**, 367–81.

Ji, W. Q., Wu, F. Y., Chung, S. L., Li, J. X. & Liu, C. Z. 2009*a*. Zircon U–Pb geochronology and Hf isotopic constraints on petrogenesis of the Gangdese batholith, southern Tibet. *Chemical Geology* **262**, 229–45.

Ji, W. Q., Wu, F. Y., Liu, C. Z. & Chung, S. L. 2009*b*. Geochronology and petrogenesis of granitic rocks in Gangdese batholith, southern Tibet. *Science in China Series D: Earth Sciences* **52**, 1240–61.

Ji, W. Q., Wu, F. Y., Liu, C. Z. & Chung, S. L. 2012. Early Eocene crustal thickening in southern Tibet: new age and geochemical constraints from the Gangdese batholith. *Journal of Asian Earth Sciences* **53**, 82–95.

Jiang, Z. Q., Wang, Q., Li, Z. X., Wyman, D. A., Tang, G. J., Jia, X. H. & Yang, Y. H. 2012. Late Cretaceous (ca. 90 Ma) adakitic intrusive rocks in the Kelu area, Gangdese belt (southern Tibet): slab melting and implications for Cu–Au mineralization. *Journal of Asian Earth Sciences* **53**, 67–81.

Kang, Z. Q., Xu, J. F., Wilde, S. A., Feng, Z. H., Chen, J. L., Wang, B. D., Fu, W. C. & Pan, H. B. 2014. Geochronology and geochemistry of the Sangri Group volcanic rocks, southern Lhasa terrane: implications for the early subduction history of the Neo-Tethys and Gangdese magmatic arc. *Lithos* **200–201**, 157–68.

Kapp, P., DeCelles, P. G., Gehrels, G. E., Heizler, M. & Ding, L. 2007. Geological records of the Lhasa-Qiangtang and Indo-Asian collisions in the Nima area of central Tibet. *Geological Society of America Bulletin* **119**, 917–33.

Kapp, P., Murphy, M. A., Yin, A., Harrison, T. M., Ding, L. & Guo, J. 2003. Mesozoic and Cenozoic tectonic evolution of the Shiquanhe area of western Tibet. *Tectonics* **22**, 1029.

Kelemen, P. B., Hart, S. R., & Bernstein, S. 1998. Silica enrichment in the continental upper mantle via melt/rock reaction. *Earth and Planetary Science Letters* **164**, 387–406.

Kimura, H., Kasahara, K. & Takeda, T. 2009. Subduction process of the Philippine Sea Plate off the Kanto district, central Japan, as revealed by plate structure and repeating earthquakes. *Tectonophysics* **472**, 18–27.

Klemd, R. 2013. Metasomatism during high-pressure metamorphism: eclogites and blueschist facies rocks. In *Metasomatism and the Chemical Transformation of Rocks* (eds D. E. Harlov & H. Austrheim), pp. 351–413. Berlin and Heidelberg: Springer.

Li, S. M., Zhu, D. C., Wang, Q., Zhao, Z., Zhang, L. L., Liu, S. A., Chang, Q. L., Lu, Y. H., Dai, J. G. & Zheng, Y. C. 2016. Slab-derived adakites and subslab asthenosphere-derived OIB-type rocks at 156 ± 2 Ma from the north of Gerze, central Tibet: records of the Bangong–Nujiang oceanic ridge subduction during the Late Jurassic. *Lithos* **262**, 456–69.

Liu, Q. S., Jiang, W., Jian, P., Ye, P. S., Wu, Z. H. & Hu, D. G. 2006. Zircon SHRIMP U-Pb age and petrochemical and geochemical features of Mesozoic muscovite granite in Ningzhong, Tibet. *Acta Petrologica Sinica* **22**, 643–52 (in Chinese with English abstract).

Liu, X. M., Gao, S., Diwu, C. R., Yuan, H. L. & Hu, Z. C. 2007. Simultaneous in-situ determination of U-Pb age and trace elements in zircon by LA-ICP-MS in 20 μm spot size. *Chinese Science Bulletin* **52**, 1257–64.

Liu, Y. S., Gao, S., Hu, Z. C., Gao, C. G., Zong, K. Q & Wang, D. B. 2010. Continental and oceanic crust recycling-induced Melt–Peridotite interactions in the Trans-North China Orogen: U–Pb dating, Hf isotopes and trace elements in zircons from Mantle Xenoliths. *Journal of Petrology* **51**, 537–71.

Lu, T. Y., He, Z. Y., Zhang, Z. M., Shui, X. F. & Yan, L. L. 2016. Magma mixing of the Nyemo post-collisional granite from the Gangdese magmatic belt, Tibet: evidence of microstructures. *Acta Petrologica Sinica* **32**, 3613–23 (in Chinese with English abstract).

Ludwig, K. R. 2003. *User's Manual for Isoplot 3.00, a Geochronological Toolkit for Microsoft Excel*. Berkeley Geochronology Center, Special Publication no. 4, 25–32.

Ma, L., Wang, B. D., Jiang, Z. Q., Wang, Q., Li, Z. X., Wyman, D. A., Zhao, S. R., Yang, J. H., Gou, G. N. & Guo, H. F. 2014. Petrogenesis of the Early Eocene adakitic rocks in the Napuri area, southern Lhasa: partial melting of thickened lower crust during slab break-off and implications for crustal thickening in southern Tibet. *Lithos* **196–197**, 321–38.

Ma, L., Wang, Q., Wyman, D. A., Li, Z. X., Jiang, Z. Q., Yang, J. H., Gou, G. N. & Guo, H. F. 2013. Late Cretaceous (100–89 Ma) magnesian charnockites with adakitic affinities in the Milin area, eastern Gangdese: partial melting of subducted oceanic crust and implications for crustal growth in southern Tibet. *Lithos* **175–176**, 315–32.

Ma, S. W., Meng, Y. K., Xu, Z. Q. & Liu, X. J. 2017. The discovery of late Triassic mylonitic granite and geologic significance in the middle Gangdese batholiths, southern Tibet. *Journal of Geodynamics* **104**, 49–64.

Macpherson, C. G., Dreher, S. T. & Thirlwall, M. F. 2006. Adakites without slab melting: high pressure differentiation of island arc magma, Mindanao, the Philippines. *Earth and Planetary Science Letters* **243**, 581–93.

Maniar, P. D. & Piccoli, P. M. 1989. Tectonic discrimination of granitoids. *Geological Society of America Bulletin* **101**, 635–43.

Meng, F. Y., Zhao, Z., Zhu, D. C., Mo, X., Guan, Q., Huang, Y., Dong, G. S, Zhou, S., DePaolo, D. J., Harrison, T., Zhang, Z. S, Liu, J. L, Liu, Y. S, Hu, Z. C. & Yuan, H. L. 2014. Late Cretaceous magmatism in Mamba area, central Lhasa subterrane: products of

https://doi.org/10.1017/S0016756817000577 Published online by Cambridge University Press

back-arc extension of Neo-Tethyan Ocean? *Gondwana Research* **26**, 505–20.

MENG, Y. K., DONG, H. W., CONG, Y., XU, Z. Q. & CAO, H. 2016a. The early-stage evolution of the Neo-Tethys ocean: evidence from granitoids in the middle Gangdese batholith, southern Tibet. *Journal of Geodynamics* **94–95**, 34–49.

MENG, Y. K., XU, Z. Q., SANTOSH, M., MA, X. X., CHEN, X. J., GUO, G. L. & LIU, F., 2016b. Late Triassic crustal growth in southern Tibet: evidence from the Gangdese magmatic belt. *Gondwana Research* **37**, 449–64.

METCALFE, I. 1996. Gondwanaland dispersion, Asian accretion and evolution of Eastern Tethys. *Australian Journal of Earth Sciences* **43**, 605–23.

METCALFE, I. 2009. Late Palaeozoic and Mesozoic tectonic and palaeogeographic evolution of SE Asia. In *Late Palaeozoic and Mesozoic Continental Ecosystems in SE Asia* (eds E. Buffetaut, G. Cuny, J. Le Loeuff and V. Suteethorn), pp. 7–23. Geological Society of London, Special Publication no. 315.

METCALFE, I. 2011. Tectonic framework and Phanerozoic evolution of Sundaland. *Gondwana Research* **19**, 3–21.

MIDDLEMOST, E. A. K. 1994. Naming materials in the magma/igneous rock system. *Earth-Science Reviews* **37**, 215–24.

MO, X. X. 2011. Magmatism and evolution of the Tibetan Plateau. *Geological Journal of China Universities* **17**, 351–67 (in Chinese with English abstract).

MO, X. X., DONG, G. C., ZHAO, Z. D., GUO, T. Y., WANG, L. L. & CHEN, T. 2005. Timing of magma mixing in the Gangdise magmatic belt during the India Asia collision: zircon SHRIMP U–Pb dating. *Acta Geologica Sinica (English Edition)* **79**, 66–76.

MO, X. X., DONG, G. C., ZHAO, Z. D., YU, X. H., SHEN, S. Y., ZHU, D. C., KE, S., ZHOU, S., WANG, L. B. & WANG, Q. L. 2013. *Tectonic–Magmatic Geological Map of Tibetan Plateau and its Adjacent Area, 1:1,500,000*. Beijing: Geological Publishing House.

NAKAMURA, H. & IWAMORI, H. 2013. Generation of adakites in a cold subduction zone due to double subducting plates. *Contributions to Mineralogy and Petrology* **165**, 1107–34.

NIU, Y. L. & BATIZA, R. 1997. Trace element evidence from seamounts for recycled oceanic crust in the eastern equatorial Pacific mantle. *Earth and Planetary Science Letters* **148**, 471–84.

NIU, Y. L., ZHAO, Z. D, ZHU, D. C. & MO, X. X. 2013. Continental collision zones are primary sites for net continental crust growth: a testable hypothesis. *Earth-Science Reviews* **127**, 96–110.

PALLARES, C., MAURY, R. C., BELLON, H., ROYER, J. Y., CALMUS, T., AGUILLÓN-ROBLES, A., COTTON, J., BENOIT, M., MICHAUD, F. & BOURGOIS, J. 2007. Slab-tearing following ridge-trench collision: evidence from Miocene volcanism in Baja California, México. *Journal of Volcanology and Geothermal Research* **161**, 95–117.

PAN, G. T., DING, J., YAO, D. S. & WANG, L. Q. 2004. *Guidebook of 1:1,500,000 Geological Map of the Qinghai–Xizang (Tibet) Plateau and Adjacent Areas*. Chengdu: Cartographic Publishing House, 148 pp.

PEACOCK, S. M., RUSHMER, T. & THOMPSON, A. B., 1994. Partial melting of subducting oceanic-crust. *Earth and Planetary Science Letters* **121**, 227–44.

PEACOCK, S. M., VAN KEKEN, P. E., HOLLOWAY, S. D., HACKER, B. R., ABERS, G. A. & FERGUSON, R. L. 2005. Thermal structure of the Costa Rica–Nicaragua subduction zone. *Physics of the Earth and Planetary Interiors* **149**, 187–200.

PERUGINI, D., POLI, G., CHRISTOFIDES, G. & ELEFTHERIADIS, G. 2003. Magma mixing in the Sithonia Plutonic Complex, Greece: evidence from mafic microgranular enclaves. *Mineralogy and Petrology* **78**, 173–200.

PETFORD, N. & ATHERTON, M. 1996. Na-rich partial melts from newly underplated basaltic crust: the Cordillera Blanca batholith, Peru. *Journal of Petrology* **37**, 1491–521.

PETRONE, C. M. & FERRARI, L. 2008. Quaternary adakite–Nb-enriched basalt association in the western Trans-Mexican Volcanic Belt: is there any slab melt evidence? *Contributions to Mineralogy and Petrology* **156**, 73–86.

PLANK, T. 2005. Constraints from thorium/lanthanumon sediment recycling at subduction zones and the evolution of the continents. *Journal of Petrology* **46**, 921–44.

PLANK, T. & LANGMUIR, C. H. 1998. The chemical composition of subducting sediment and its consequences for the crust and mantle. *Chemical Geology* **145**, 325–94.

QIU, J. S., WANG, R. Q., ZHAO, J. L. & YU, S. B. 2015. Petrogenesis of the Early Jurassic gabbro-granite complex in the middle segment of the Gangdese belt and its implications for tectonic evolution of Neo-Tethys: a case study of the Dongga pluton in Xigaze. *Acta Petrologica Sinica* **31**, 3569–80 (in Chinese with English abstract).

QIU, R. Z., ZHOU, S., DENG, J. F., LI, J. F., XIAO, Q. H. & CAI, Z. Y. 2004. Dating of gabbro in the Shemalagou ophiolite in the western segment of the Bangong Co-Nujiang ophiolite belt, Tibet – with a discussion of the age of the Bangong Co-Nujiang ophiolite belt. *Geology in China* **31**, 262–8 (in Chinese with English abstract).

QU, X. M., XIN, H. B. & XU, W. Y. 2007. Collation of age of ore-hosting volcanics in Xiongcun superlarge Cu–Au deposit on basis of three zircon U–Pb SHRIMP ages. *Mineral Deposits* **26**, 512–8 (in Chinese with English abstract).

RAPP, R., SHIMIZU, N., NORMAN, M. & APPLEGATE, G. 1999. Reaction between slab-derived melts and peridotite in the mantle wedge: experimental constraints at 3.8 GPa. *Chemical Geology* **160**, 335–56.

RAPP, R. P. & WATSON, E. B. 1995. Dehydration melting of metabasalt at 8–32 kbar: implications for continental growth and crust–mantle recycling. *Journal of Petrology* **36**, 891–931.

RIBEIRO, J. M., MAURY, R. C. & GRÉGOIRE, M. 2016. Are Adakites slab melts or high-pressure fractionated mantle melts? *Journal of Petrology* **57**, 839–62.

RODRÍGUEZ, C., SELLÉS, D., DUNGAN, M., LANGMUIR, C. & LEEMAN, W. 2007. Adakitic dacite formed by intracrustal crystal fractionation of water-rich parent magmas at Nevado de Longavi Volcano (36.2° S; Andean Southern Volcanic Zone, Central Chile). *Journal of Petrology* **48**, 2033–61.

ROLLINSON, H. R. 1993. Discriminating between tectonic environments using geochemical data. In *Using Geochemical Data: Evaluation, Presentation, Interpretation*, pp. 171–214. Harlow: Longman Scientific & Technical.

SAJONA, F. G., MAURY, R. C., BELLON, H., COTTON, J., DEFANT, M. J., PUBELLIER, M. & RANGIN, C. 1993. Initiation of subduction and the generation of slab melts in western and eastern Mindanao, Philippines. *Geology* **21**, 1007–10.

SCHÄRER, U., XU, R. H. & ALLEGRE, C. J. 1984. U–Pb geochronology of Gangdese (Transhimalaya) plutonism in the Lhasa–Xigaze region, Tibet. *Earth and Planetary Science Letters* **69**, 311–20.

SEN, C. & DUNN, T. 1994. Experimental modal metasomatism of a spinel lherzolite and the production of

amphibole-bearing peridotite. *Contributions to Mineralogy and Petrology* **119**, 422–32.
SENGÖR, A. M. C., ALTLNER, D., CIN, A., USTAIIMER, T. & HSTI, K. J. 1988. Origin and assembly of the Tethyside orogenic collage at the expense of Gondwana Land. In *Gondwana and Tethys* (ed. M. G. Audley-Charles), pp. 119–81. Geological Society of London, Special Publication no. 37, 119–81.
SHELLNUTT, J. G., JAHN, B. M. & DOSTAL, J. 2010. Elemental and Sr–Nd isotope geochemistry of microgranular enclaves from peralkaline A-type granitic plutons of the Emeishan large igneous province, SW China. *Lithos* **119**, 34–46.
SHUI, X. F., HE, Z. Y., ZHANG, Z. M. & LU, T. Y. 2016. Magma origin of Early Jurassic tonalites in the Eastern Gangdese Magmatic Belt, southern Tibet and its implications for the crustal evolution of the Lhasa Terrane. *Acta Geologica Sinica* **90**, 3129–52 (in Chinese with English abstract).
SÖDERLUND, U., PATCHETT, P. J., VERVOORT, J. D. & ISACHSEN, C. E. 2004. The ^{176}Lu decay constant determined by Lu–Hf and U–Pb isotope systematics of Precambrian mafic intrusions. *Earth and Planetary Science Letters* **219**, 311–24.
SONG, S. W., LIU, Z., ZHU, D. C., WANG, Q., ZHANG, L. X., ZHANG, L. L. & ZHAO, Z. D. 2014. Zircon U–Pb chronology and Hf isotope of the Late Triassic andesitic magmatism in Dajiacuo, Tibet. *Acta Petrologica Sinica* **30**, 3100–12 (in Chinese with English abstract).
SPARKS, R. S. J. & MARSHALL, L. A. 1986. Thermal and mechanical constraints on mixing between mafic and silicic magmas. *Journal of Volcanology and Geothermal Research* **29**, 99–124.
STERN, C. R. & KILIAN, R. 1996. Role of the subduction slab, mantle wedge and continental crust in the generation of adakites from the Andean Austral Volcanic Zone. *Contributions to Mineralogy and Petrology* **123**, 263–81.
SUN, S. S. & MCDONOUGH, W. F. 1989. Chemical and isotopic systematics of oceanic basalts: implications for mantle composition and processes. In *Magmatism in the Ocean Basins* (eds A. D. Saunders & M. J. Norry), pp. 313–45. Geological Society of London, Special Publication no. 42.
TAYLOR, S. R. & MCLENNAN, S. M. 1985. *The Continental Crust: Its Composition and Evolution*. London: Blackwell, 328 pp..
THORKELSON, D. J. & BREITSPRECHER, K. 2005. Partial melting of slab window margins: genesis of adakitic and non-adakitic magmas. *Lithos* **79**, 25–41.
VAN KEKEN, P. E., HACKER, B. R., SYRACUSE, E. M. & ABERS, G. A. 2011. Subduction factory: 4. Depth-dependent flux of H_2O from subducting slabs worldwide. *Journal of Geophysical Research: Solid Earth* **116**, B01401.
VERNON, R. 1984. Microgranitoid enclaves in granites–globules of hybrid magma quenched in a plutonic environment. *Nature* **309**, 438–9.
WAIGHT, T. E., MAAS, R. & NICHOLLS, I. A. 2000. Fingerprinting feldspar phenocrysts using crystal isotopic composition stratigraphy: implications for crystal transfer and magma mingling in S-type granites. *Contributions to Mineralogy and Petrology* **139**, 227–39.
WANG, Q., LI, X. H., JIA, X. H., WYMAN, D., TANG, G. J., LI, Z. X., MA, L., YANG, Y. H., JIANG, Z. Q. & GOU, G. N. 2012. Late Early Cretaceous adakitic granitoids and associated magnesian and potassium-rich mafic enclaves and dikes in the Tunchang–Fengmu area, Hainan Province (South China): partial melting of lower crust and mantle, and magma hybridization. *Chemical Geology* **328**, 222–43.
WANG, C., DING, L., ZHANG, L. Y., KAPP, P., PULLEN, A. & YUE, Y. H. 2016. Petrogenesis of Middle-Late Triassic volcanic rocks from the Gangdese belt, southern Lhasa terrane: Implications for early subduction of Neo-Tethyan oceanic lithosphere. *Lithos* **262**, 320–333.
WEI, Y. Q. 2014. The geochronology, geochemistry and petrogenesis of the volcanic rocks of Yeba Formation, southern Tibet. Master thesis, China University of Geosciences, Beijing. Published thesis.
WEN, D. R., CHUNG, S. L., SONG, B., IIZUKA, Y., YANG, H. J., JI, J. Q., LIU, D. Y. & GALLET, S. 2008a. Late Cretaceous Gangdese intrusions of adakitic geochemical characteristics, SE Tibet: petrogenesis and tectonic implications. *Lithos* **105**, 1–11.
WEN, D. R., LIU, D., CHUNG, S. L., CHU, M. F., JI, J., ZHANG, Q., SONG, B., LEE, T. Y., YEH, M. W. & LO, C. H. 2008b. Zircon SHRIMP U–Pb ages of the Gangdese Batholith and implications for Neotethyan subduction in southern Tibet. *Chemical Geology* **252**, 191–201.
XU, W., GAO, S., WANG, Q., WANG, D. & LIU, Y. 2006. Mesozoic crustal thickening of the eastern North China craton: evidence from eclogite xenoliths and petrologic implications. *Geology* **34**, 721–4.
XU, W. C., ZHANG, H. F., LUO, B. J., GUO, L. & YANG, H. 2015. Adakite-like geochemical signature produced by amphibole-dominated fractionation of arc magmas: an example from the Late Cretaceous magmatism in Gangdese belt, south Tibet. *Lithos* **232**, 197–210.
YANG, J. H., WU, F. Y., WILDE, S., XIE, L. W., YANG, Y. H. & LIU, X. M. 2007. Tracing magma mixing in granite genesis: in situ U–Pb dating and Hf-isotope analysis of zircons. *Contributions to Mineralogy and Petrology* **153**, 177–90.
YANG, Z. M., HOU, Z. Q., JIANG, Y. F., ZHANG, H. R. & SONG, Y. C. 2011. Sr-Nd-Pb and zircon Hf isotopic constraints on petrogenesis of the Late Jurassic granitic porphyry at Qulong, Tibet. *Acta Petrologica Sinica* **27**, 2003–10 (in Chinese with English abstract).
YIN, A. & HARRISON, T. M. 2000. Geologic evolution of the Himalayan–Tibetan Orogen. *Annual Review of Earth and Planetary Sciences* **28**, 211–80.
YOGODZINSKI, G. M. & KELEMEN, P. B. 1998. Slab melting in the Aleutians: implications of an ion probe study of clinopyroxene in primitive adakite and basalt. *Earth and Planetary Science Letters* **158**, 53–65.
YOGODZINSKI, G., LEES, J., CHURIKOVA, T., DORENDORF, F., WOERNER, G. & VOLYNETS, O. 2001. Geochemical evidence for the melting of subducting oceanic lithosphere at plate edges. *Nature* **409**, 500–4.
ZHANG, H. F., XU, W. C., GUO, J. Q., ZONG, K. Q., CAI, H. M. & YUAN, H. L. 2007a. Zircon U–Pb and Hf isotopic composition of deformed granite in the southern margin of the Gangdese belt, Tibet: evidence for early Jurassic subduction of Neo-Tethyan oceanic slab. *Acta Petrologica Sinica* **23**, 1347–53 (in Chinese with English abstract).
ZHANG, H. F., XU, W. C., GUO, J. Q., ZONG, K. Q., CAI, H. M. & YUAN, H. L. 2007b. Indosinian orogenesis of the gangdise terrane: evidences from zircon U-Pb dating and petrogenesis of granitoids. *Earth Science – Journal of China University of Geoscience* **32**, 155–66 (in Chinese with English abstract).
ZHANG, Z. M., ZHAO, G. C., SANTOSH, M., WANG, J. L., DONG, X. & SHEN, K. 2010. Late Cretaceous charnock-

https://doi.org/10.1017/S0016756817000577 Published online by Cambridge University Press

ite with adakitic affinities from the Gangdese batholith, southeastern Tibet: evidence for Neo-Tethyan mid-ocean ridge subduction? *Gondwana Research* **17**, 615–31.

Zhao, Z. H., Xiong, X. L., Wang, Q., Wyman, D. A., Bao, Z. W., Bai, Z. H. & Qiao, Y. L. 2008. Underplating related adakites in Xinjiang Tianshan, China. *Lithos* **102**, 374–91.

Zheng, Y. C., Hou, Z. Q., Li, Q. Y., Sun, Q. Z., Liang, W., Fu, Q., Li., W. & Huang, K. X. 2012. Origin of Late Oligocene adakitic intrusives in the southeastern Lhasa terrane: evidence from in situ zircon U–Pb dating, Hf–O isotopes, and whole-rock geochemistry. *Lithos* **148**, 296–311.

Zhong, H. T., Dai, J. G., Wang, C. S., Li, Y. L. & Wei, Y. S. 2016. Middle Jurassic-Early Cretaceous radiolarian assemblages of the western Yarlung Zangbo Suture Zone: implications for the evolution of the Neo-Tethys. *Geoscience Frontiers*, Published online 15 October 2016. https://doi.org/10.1016/j.gsf.2016.09.006.

Zhu, D. C., Pan, G. T., Chung, S. L., Liao, Z. L., Wang, L. Q. & Li, G. M. 2008. SHRIMP zircon age and geochemical constraints on the origin of lower Jurassic volcanic rocks from the Yeba formation, Southern Gangdese, south Tibet. *International Geology Review* **50**, 442–71.

Zhu, D. C., Wang, Q., Zhao, Z. D., Chung, S. L., Cawood, P. A., Niu, Y. L., Liu, S. A., Wu, F. Y. & Mo, X. X. 2015. Magmatic record of India–Asia collision. *Scientific Reports* **5**, 14289.

Zhu, D. C., Zhao, Z. D., Niu, Y. L., Mo, X. X., Chung, S. L. & Hou, Z. Q. 2011a. The Lhasa Terrane: record of a microcontinent and its histories of drift and growth. *Earth and Planetary Science Letters* **301**, 241–55.

Zhu, D. C., Zhao, Z. D., Niu, Y. L., Dilek, Y. & Mo, X. X., 2011b. Lhasa terrane in southern Tibet came from Australia. *Geology* **39**, 727–30.

Zhu, D. C., Zhao, Z. D., Pan, G. T., Lee, H. Y., Kang, Z. Q., Liao, Z. L., Wang, L. Q., Li, G. M., Dong, G. C. & Liu, B. 2009. Early Cretaceous subduction-related adakite-like rocks of the Gangdese Belt, southern Tibet: products of slab melting and subsequent melt–peridotite interaction? *Journal of Asian Earth Sciences* **34**, 298–309.